iScience

CellPress
OPEN ACCESS

Article

Functional regulation of microglia by vitamin B12 alleviates ischemic stroke-induced neuroinflammation in mice

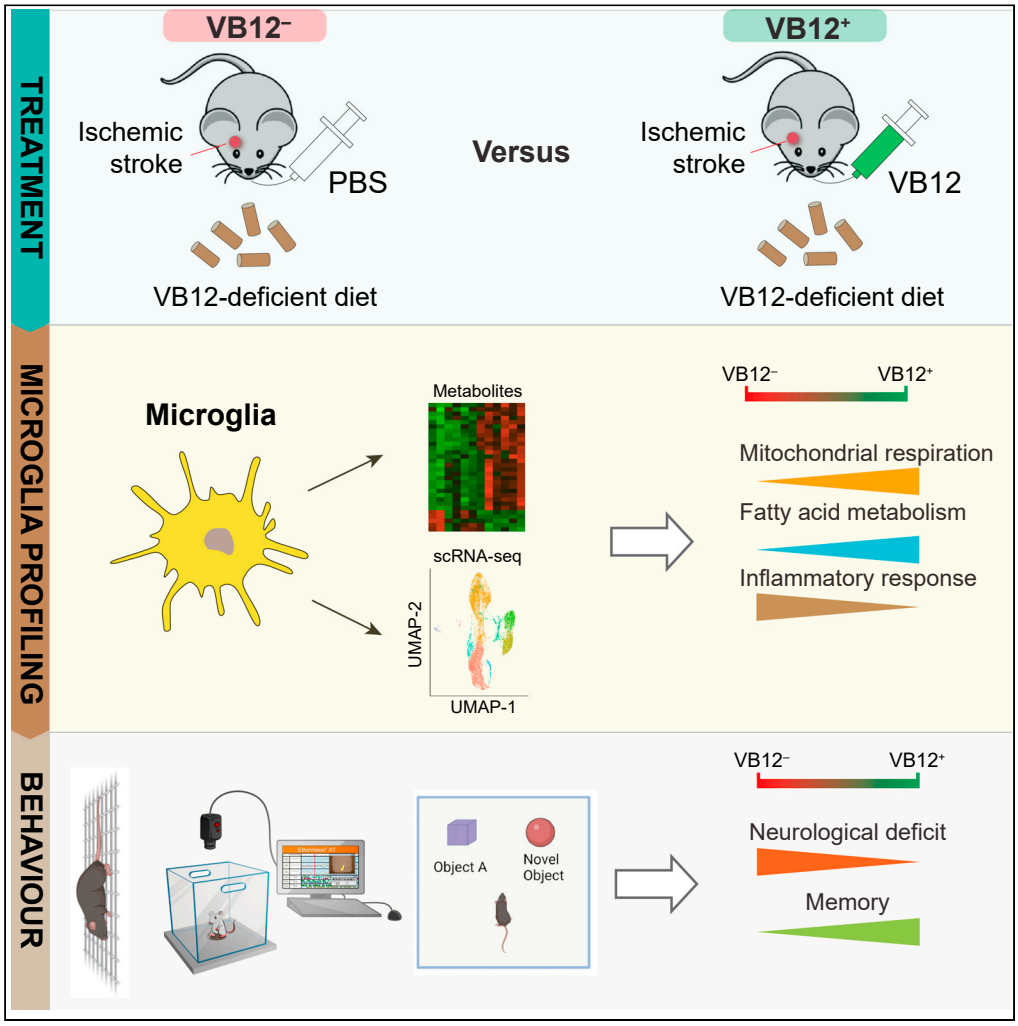

Yong Ge, Changjun Yang, Mojgan Zadeh, ..., Jonathan Larochelle, Eduardo Candelario-Jalil, Mansour Mohamadzadeh

gey@uthscsa.edu (Y.G.)
Zadehm@uthscsa.edu (M.M.)

Highlights

VB12 supports the activation of homeostatic microglia

VB12 functionally programs the metabolic circuits of microglia during homeostasis and ischemic stroke

Single-cell transcriptomics reveals differential regulation of microglia subsets by VB12

VB12 reduces cerebral injury and improves long-term neurobehavioral function post-stroke

Ge et al., iScience 27, 109480
April 19, 2024
https://doi.org/10.1016/j.isci.2024.109480

iScience

CellPress
OPEN ACCESS

Article

Functional regulation of microglia by vitamin B12 alleviates ischemic stroke-induced neuroinflammation in mice

Yong Ge,[1,*] Changjun Yang,[2] Mojgan Zadeh,[1] Shane M. Sprague,[3] Yang-Ding Lin,[1] Heetanshi Sanjay Jain,[1] Brenden Fitzgerald Determann II,[1] William H. Roth,[4] Juan Pablo Palavicini,[1] Jonathan Larochelle,[2] Eduardo Candelario-Jalil,[2] and Mansour Mohamadzadeh[1,5,*]

SUMMARY

Ischemic stroke is the second leading cause of death and disability worldwide, and efforts to prevent stroke, mitigate secondary neurological damage, and promote neurological recovery remain paramount. Recent findings highlight the critical importance of microbiome-related metabolites, including vitamin B12 (VB12), in alleviating toxic stroke-associated neuroinflammation. Here, we showed that VB12 tonically programmed genes supporting microglial cell division and activation and critically controlled cellular fatty acid metabolism in homeostasis. Intriguingly, VB12 promoted mitochondrial transcriptional and metabolic activities and significantly restricted stroke-associated gene alterations in microglia. Furthermore, VB12 differentially altered the functions of microglial subsets during the acute phase of ischemic stroke, resulting in reduced brain damage and improved neurological function. Pharmacological depletion of microglia before ischemic stroke abolished VB12-mediated neurological improvement. Thus, our preclinical studies highlight the relevance of VB12 in the functional programming of microglia to alleviate neuroinflammation, minimize ischemic injury, and improve host neurological recovery after ischemic stroke.

INTRODUCTION

Ischemic stroke, which accounts for approximately 85% of all strokes, occurs as a result of insufficient cerebral blood flow to the brain, resulting in irreversible tissue damage and neurological deficits or death.[1] The identification of risk factors for ischemic stroke has led to the development of medical and surgical prophylactic interventions that have reduced the incidence of stroke.[2] Despite these advances, stroke remains a major contributor to the global burden of disease.[2] In 2016, stroke was the second leading cause of death worldwide, claiming the lives of approximately 5.5 million people and an estimated 80 million of survivors struggle with the detrimental effects of stroke.[3] Currently, increased scientific efforts to mechanistically understand the pathophysiology of stroke and curb the spread of this disease are of paramount importance.[4] Given the ubiquity of stroke, identifying reversible risk factors or new therapeutic targets will have a crucial impact on the global burden of disease.

Ischemic stroke, which accounts for approximately 85% of all strokes, occurs as a result of insufficient cerebral blood flow to the brain, triggering irreversible tissue injury and neurological deficits or death.[1] The identification of risk factors for ischemic stroke has led to the development of medical and surgical prophylactic interventions, which have reduced stroke incidence.[2] Despite these advances, stroke remains a leading contributor to the global disease burden.[2] In 2016, stroke was the second leading cause of death worldwide, claiming the lives of approximately 5.5 million people along with an estimated 80 million survivors contending with deleterious effects of stroke.[3] Currently, intensified scientific efforts to mechanistically understand stroke pathophysiology and stem the tide of this disease are of the utmost importance.[4] Considering the ubiquity of stroke, identifying reversible risk factors or new therapeutic targets will have a crucial impact on the global disease burden.

Vitamin B12 (VB12) is a necessary cofactor for methionine synthase and its deficiency leads to the accumulation of atherogenic homocysteine, a well-known risk factor for ischemic stroke. As previously discussed,[5] although large-scale clinical trials[6] showed mixed results in reducing stroke while replenishing B vitamins,[7] a meta-analysis that excluded patients with impaired renal function, showed a clear and convincing benefit.[8] A subgroup analysis demonstrated VB12 combined with B vitamins dramatically reduced stroke, myocardial infarction, and vascular death by 34% in patients without renal impairment.[9] It was reasonably postulated that accumulation of the toxic VB12 byproduct

[1]Department of Microbiology, Immunology & Molecular Genetics, University of Texas Health, San Antonio, TX, USA
[2]Department of Neuroscience, McKnight Brain Institute, University of Florida, Gainesville, FL, USA
[3]Department of Neurosurgery, University of Texas Health, San Antonio, TX, USA
[4]Department of Neurology, University of Chicago Medical Center, Chicago, IL, USA
[5]Lead contact
*Correspondence: gey@uthscsa.edu (Y.G.), Zadehm@uthscsa.edu (M.M.)
https://doi.org/10.1016/j.isci.2024.109480

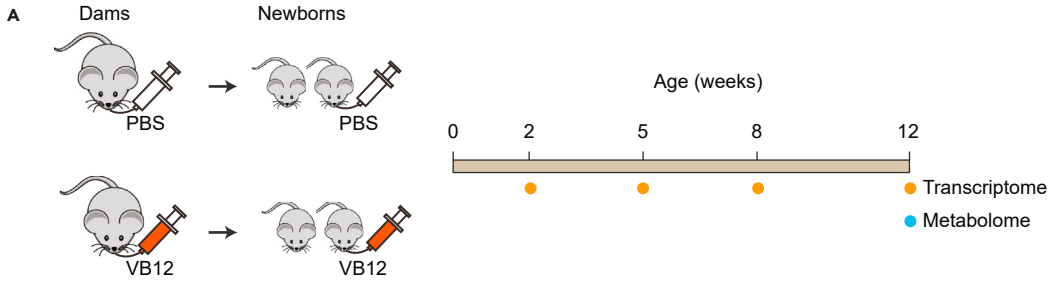
A
Dams
Newborns
PBS
PBS
VB12
VB12
Age (weeks)
0
2
5
8
12
Transcriptome
Metabolome

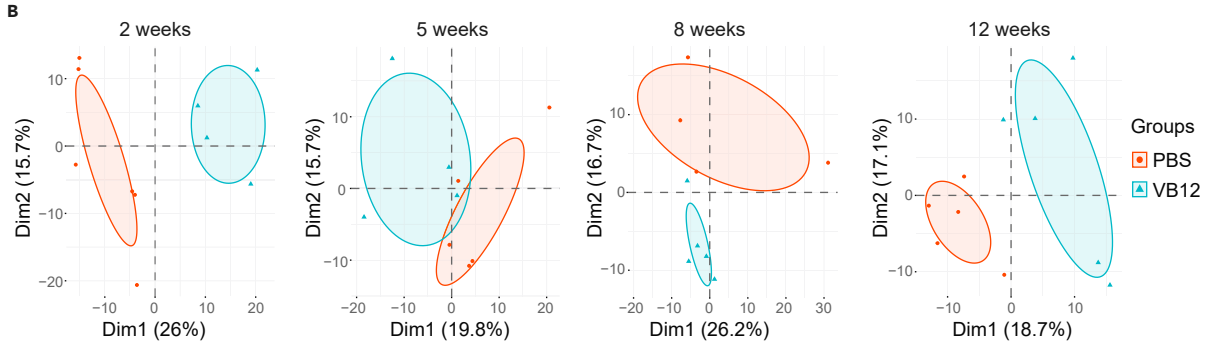
B
2 weeks
5 weeks
8 weeks
12 weeks
Dim2 (15.7%)
Dim1 (26%)
Dim2 (15.7%)
Dim1 (19.8%)
Dim2 (16.7%)
Dim1 (26.2%)
Dim2 (17.1%)
Dim1 (18.7%)
Groups
PBS
VB12

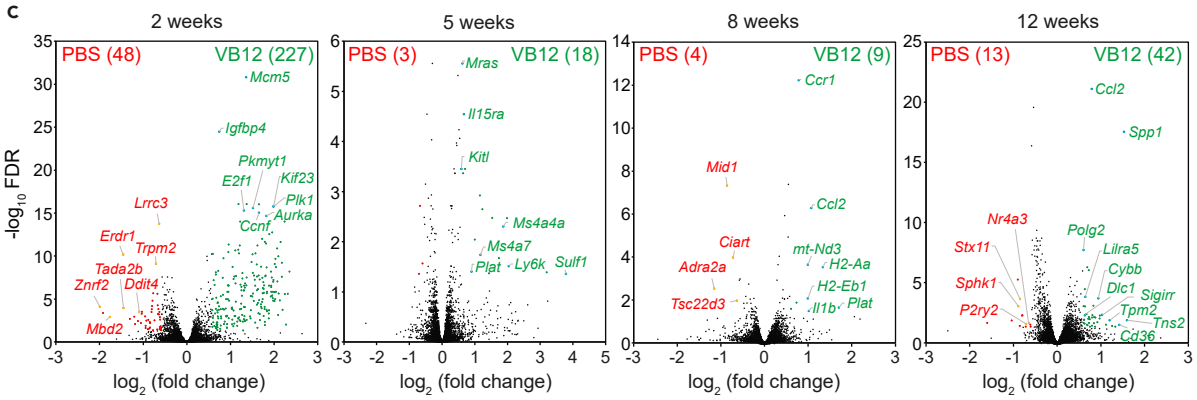
C
2 weeks
5 weeks
8 weeks
12 weeks
PBS (48)
VB12 (227)
PBS (3)
VB12 (18)
PBS (4)
VB12 (9)
PBS (13)
VB12 (42)
-log10 FDR
log2 (fold change)
Mcm5
Igfbp4
Pkmyt1
E2f1
Kif23
Plk1
Aurka
Ccnf
Lrrc3
Erdr1
Trpm2
Tada2b
Znrf2
Ddit4
Mbd2
Mras
Il15ra
Kitl
Ms4a4a
Ms4a7
Plaur
Ly6k
Sulf1
Ccr1
Mid1
Ccl2
Ciart
mt-Nd3
H2-Aa
Adra2a
H2-Eb1
Tsc22d3
Il1b
Plat
Ccl2
Spp1
Nr4a3
Polg2
Stx11
Lilra5
Cybb
Sphk1
Dlc1
Sigirr
P2ry2
Tpm2
Tns2
Cd36

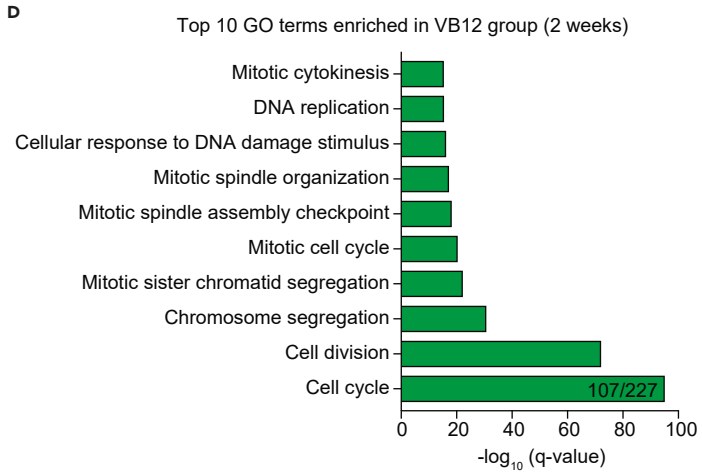
D
Top 10 GO terms enriched in VB12 group (2 weeks)
Mitotic cytokinesis
DNA replication
Cellular response to DNA damage stimulus
Mitotic spindle organization
Mitotic spindle assembly checkpoint
Mitotic cell cycle
Mitotic sister chromatid segregation
Chromosome segregation
Cell division
Cell cycle
107/227
-log10 (q-value)

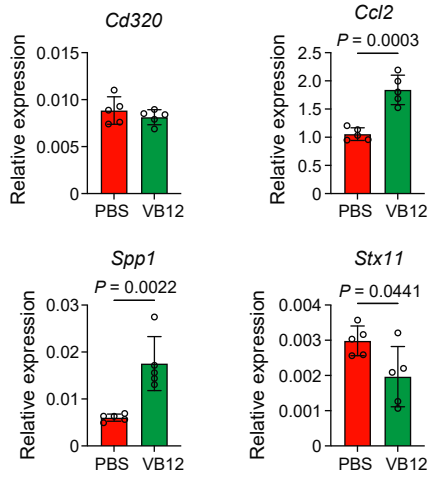
E
Cd320
Ccl2
P = 0.0003
Spp1
P = 0.0022
Stx11
P = 0.0441
Relative expression
PBS
VB12

Figure 1. VB12 regulates the transcriptional activities of microglia at homeostasis

(A) Experimental scheme. Groups of pregnant C57BL/6 dams fed a VB12-deficient diet were gavaged with VB12 or PBS twice a week until the delivery of their newborns. Newborn mice were continuously kept on the same VB12-deficient diet and gavaged with VB12 or PBS twice a week for 12 weeks. Mice were euthanized at 2, 5, 8, and 12 weeks of age to FACS-sort microglia for bulk RNA-seq. Untargeted cellular metabolomes were analyzed for microglia isolated from 12-week-old mice.

(B) Principal component analysis (PCA) plot of transcriptomes of microglia isolated from VB12- and PBS-gavaged mice at 2, 5, 8 and 12 weeks of age (n = 4–6/group).

(C) RNA-seq results depicted as volcano plots showing the differentially expressed genes (DEGs) (fold change >1.5, FDR <0.05). The number of DEGs enriched in each group is shown in parentheses.

(D) DAVID Gene Ontology (GO) analysis, related to biological process, showing upregulated pathways in VB12 group compared to PBS control at 2 weeks of age. About 47.1% of total enriched genes (107/227) were associated with cell cycle activity.

(E) RT-qPCR validation of representative DEGs in 12-week-old mice gavaged with VB12 or PBS. Statistics was determined by Unpaired *t*-test.

thiocyanate resulted in adverse outcomes in patients with renal impairment, which obscured the benefit of VB12 in intervention arms.[8] While the benefit of VB12 in reducing ischemic stroke is related to its ability to lower homocysteine, the myriad roles of VB12 in fortifying cellular homeostasis challenge the assumption that its homocysteine-lowering roles are the only means by which VB12 exerts neuroprotective effects on the subject of ischemic stroke. Furthermore, data obtained from the clinical trials do not provide crucial insights into the underlying mechanisms to rationally support B vitamin intervention beyond targeted homocysteine reduction. Thus, preclinical studies are still needed to serve as an essential precursor to clinical trials to mechanistically investigate the interplay of VB12 in cellular programs and potentially discover new targets to reduce ischemic injury with a wider effective therapeutic window and reach a larger stroke population.

In humans, VB12 binds to intrinsic factor (IF) forming an IF-VB12 complex that is recognized by its receptors (e.g., cubilin)[10,11] and internalized by ileal epithelial cells (iECs).[11] iECs then release VB12 conjugated with transcobalamin into the systemic circulation and across the blood-brain barrier to be captured by immune cells,[12] including microglia expressing the CD320 receptor.[13] VB12 critically supports cytoplasmic methionine synthase and mitochondrial methylmalonyl-CoA mutase,[12] and its deficiency can cause megaloblastic anemia and neuropsychiatric complications, potentially manifesting in severe neurological disease and death.[14,15] VB12 also exerts antioxidant and anti-inflammatory effects in a homocysteine-independent manner to crucially protect against glutamate-induced neurotoxicity,[16] which, if uncontrolled, impairs mitochondrial homeostasis and induces cell apoptosis.[17,18] Recently, we have also shown that VB12 functionally regulates iECs and gut microbiome to synergistically resist pathogenic inflammation.[19] Furthermore, VB12 contributes to intestinal homeostasis[19,20] and ameliorates neurological deficits after ischemic stroke.[21,22] These parallel findings suggest a possible role for VB12 in gut-brain cross-talk during ischemic stroke, which warrants further mechanistic elucidation.

Both central and systemic inflammation progressively exacerbate the severity of stroke. Microglia, the brain-resident macrophages, play a critical role in controlling neuroinflammation after ischemic stroke. Microglia originated from erythromyeloid progenitor cells in the embryonic yolk sac migrate into the brain parenchyma and branch out completely there.[23] These cells critically control satiety, promote memory, modify pain responses, survey the central nervous system (CNS) to repair CNS tissue damage and clear dysfunctional synaptic neurons to support neural signaling and functional connectivity.[24,25] Microglia can also adopt diverse phenotypes that either exacerbate pathological ischemic stroke progression[26] or protect against stroke-induced neuroinflammation.[27] To further elucidate microglial physiology in homeostasis and during ischemic stroke, we investigated the relevance of VB12 in functionally supporting microglial programs to limit stroke-associated neuroinflammation. Our results conspicuously show that VB12 mechanistically supports microglia, suggesting that this crucial cofactor is a clinically promising candidate for protecting hosts from ischemic stroke.

RESULTS

VB12 regulates microglial transcriptomes

The brain microglia are sentinel cells involved in swiftly regulating cerebral homeostasis and tissue repair during neural injury and neurodegeneration.[28] To elucidate the importance of VB12 in the functional regulation of microglia, groups of mice fed a VB12-deficient diet were gavaged with VB12 or PBS and subsequently euthanized at 2, 5, 8, and 12 weeks of age to FACS-sort microglia for bulk RNA-seq analysis (Figure 1A). Obtained data showed that VB12 modified microglial transcriptomes, resulting in separations of the global transcriptomes from the VB12-deficient group (Figure 1B). Differential expression analysis revealed dynamic gene expression profiles at different ages. In 2-week-old mice, there was a total of 275 differentially expressed genes (DEGs), with VB12 mainly supporting genes associated with cell cycle and cell division (e.g., *Mcm5*, *Igfbp4*, *E2f1*, and *Ccnf*) and suppressing genes involved in inflammation (*Trpm2*), apoptosis (*Erdr1* and *Znrf2*) and cellular stress (*Ddit4*) (Figures 1C and 1D). After weaning, VB12 mice exhibited an activated microglial phenotype, as evidenced by upregulated genes involved in cell differentiation (*Mras*), migration (*Plat* and *Kitl*), and maturation (*Ms4a7*) (5 weeks) as well as the enrichment of activation-related transcripts (*Ccr1*, *Ccl2*, *Il1b*, *H2-Aa*, and *H2-Eb1*) (8 weeks). At 12 weeks of age, VB12 increased microglial expression of *Lilr5* and *Tns2*, which are known to regulate leukocyte activation and migration, as well as the ROS-related *Cybb* and *Spp1*, required for microglial synaptic pruning (Figure 1C). In addition, the expression of *Ccl2* and the scavenger receptor *Cd36* was also increased by VB12. Importantly, VB12-mediated microglial activation was tightly controlled as these cells were also enriched in *Sigirr*, which has the ability to curb the inflammatory response and limit the expression of *Sphk1*, potentially controlling the expression of proinflammatory cytokines and nitric oxide in microglia (Figures 1C and 1E). Together, these data highlight the significance of VB12 in maintaining an activated state of developing microglia, which contributes to maintaining cerebral homeostasis.

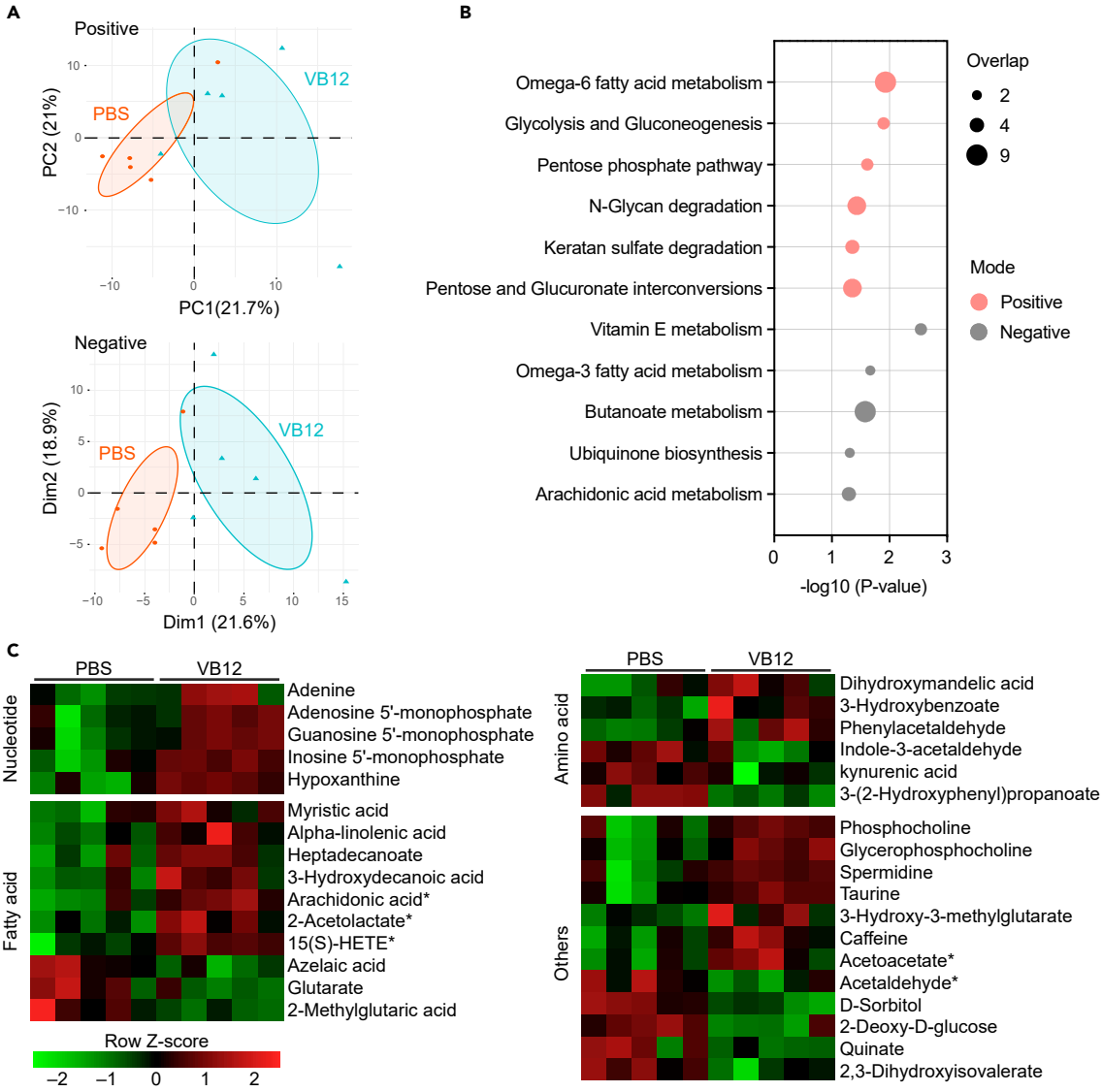

Figure 2. VB12 supports the metabolic programming of microglia

(A) PCA plots of metabolite features identified by positive or negative ionization in microglia isolated from mice gavaged with VB12 or PBS for 12 weeks (n = 5/group).

(B) Significant metabolic pathways in microglia of VB12-gavaged mice compared to PBS controls, obtained from positive or negative ionization. The overlapped size indicates the number of significant metabolic features mapped to corresponding pathways.

(C) Heatmap of significantly enriched metabolites in microglia comparing VB12 with PBS group. Metabolite identification was performed through reference to the metabolite library, curated by running each standard. Metabolites labeled with asterisks (*) were identified based on their enrichment in significant metabolic pathways and the *m/z* match.

VB12 supports microglial metabolomes

Untargeted cellular metabolomic profiling demonstrated a distinct metabolic program of microglia isolated from VB12-deficient mice compared to VB12-treated animals (Figure 2A). The balance between omega-6 and omega-3 fatty acids is an important factor in brain development and in reducing the risk of neurodegenerative diseases.[29] Notably, VB12-deficiency disrupted this balance (Figure 2B), resulting in reduced levels of arachidonic acid, its precursor alpha-linolenic acid and its derivative 15(S)-HETE (Figure 2C). VB12 also heightened nucleotide metabolism in microglia with increased levels of adenine, adenosine 5′-monophosphate, guanosine 5′-monophosphate, and inosine 5′-monophosphate (Figure 2C), potentially providing metabolic substrates to meet the increased demands to cover cell activation.[30] Interestingly, taurine and caffeine, previously shown to ameliorate reactive microglia under neuroinflammatory conditions,[31,32] were increased in VB12 mice, which also had elevated levels of antioxidant spermidine. Furthermore, phosphocholine and glycerophosphocholine, the

two major choline metabolites that facilitate the biosynthesis of the neurotransmitter acetylcholine,[33] were significantly enriched in VB12 mice. Interestingly, the neurotoxic metabolites, including kynurenic acid and quinate, were significantly reduced by VB12 (Figure 2C). These results indicate that VB12 plays a role in facilitating metabolic programming and cellular fitness of microglia.

VB12 ameliorates stroke-induced brain injury

Ischemic stroke is a potentially fatal neurological disease characterized by primary ischemic injury followed by inflammatory and oxidative secondary brain injury. Microglia are the main triggers of deleterious neuroinflammation after cerebral ischemia, but can also adopt neuroprotective immunoregulatory phenotypes that promote the resolution of inflammation.[34] Having demonstrated VB12-dependent regulation of microglia in the homeostatic state, we subsequently examined whether VB12 also functionally regulates the microglial response to induced ischemic stroke (Figure 3A). Compared to VB12 mice, VB12-deficient mice exhibited larger infarct sizes (Figures 3B and 3C) and worsened neurological deficits 24 h post-stroke injury (Figure 3D). To elaborate on these findings, we analyzed the metabolomes of microglia isolated 24 h poststroke from VB12-administrated and VB12-deficient mice. Here, VB12-deficiency markedly impaired the metabolic circuits in microglia (Figure 4A). Regulation of glutamate levels in microglia significantly supports mitochondrial oxidative metabolism and highly contributes to microglia-neuron communication.[35] Glutamate metabolism was one of the most severely impaired metabolic pathways due to VB12-deficiency (Figure 4B). Accordingly, microglia derived from VB12-deficient mice demonstrated reduced glutamate and glutamine compared to the VB12 group (Figure 4C). Furthermore, glycerophosphocholine and choline, a precursor for acetylcholine, were significantly attenuated in microglia from VB12-deficient mice (Figure 4C). Importantly, microbially derived butyrate, which is known to enhance neuroprotective microglia against stroke,[36] was significantly enriched in microglia of VB12 mice. In contrast, VB12-deficiency decreased metabolites related to the tricarboxylic acid (TCA) cycle (e.g., malate), nucleotide metabolism (e.g., adenine and guanine), and amino acid metabolism (e.g., arginine and proline) (Figures 4B and 4C). Furthermore, VB12-deficiency reduced the anti-inflammatory methyl jasmonate and increased N-(omega)-hydroxyarginine (Figure 4C), which may facilitate the biosynthesis of the proinflammatory vasodilator nitric oxide.[37] In addition, VB12-deficiency also impaired the porphyrin metabolic pathway (Figure 4B), which produces heme and accordingly reduces coproporphyrinogen and 5-aminolevulinate (Figure 4C), the precursors of heme biosynthesis. These results demonstrate the impactful relevance of VB12 in controlling microglia metabolism to limit stroke-related brain injury.

VB12 transcriptionally restricts microglia response to stroke

Our previous results have revealed that stroke affected host ileal epithelial activities within 1 day post-stroke.[38] Thus, we next analyzed the bulk transcriptomes of microglia derived from VB12 and PBS mice 1 day after MCAO. Here, VB12-deficiency profoundly affected microglial transcriptomes (Figure 5A), resulting in a total of 665 DEGs between the two groups of mice (Figure 5B). The key DEGs enriched in VB12 mice included those related to lipid metabolism (e.g., *Apob* and *Apod*), immediate-early response genes (*Ier2* and *Ier5*) that regulate cell differentiation, microglia-specific *P2ry13*, which controls hippocampal neurogenesis, as well as transcripts negatively associated with inflammatory response and microglial hyperactivation (e.g., *Mrc2*, *Tgfbr2*, *Atf3, and Cx3cr1*). The expression of *Ccl2* and *Lilra5*, enriched in the homeostatic microglia of VB12 mice (Figure 1C), was also maintained after ischemic stroke (Figure 5B). In contrast, VB12-deficiency primarily activated genes that exacerbate neuroinflammation, including *Ninj1*, *Sphk1*, *Mlkl*, *Htr2b*, and *Cx3cl3*. Furthermore, platelet factor 4 (*Pf4*), platelet-derived growth factor (*Ppbp*) and the platelet-activating factor receptor (*Ptafr*) as well as *Ecm1* suppressing TGFβ signaling were strongly activated in microglia by VB12-deficiency (Figure 5B).

To gain further insights into the interplay of VB12 in regulating the expression of stroke-associated microglial signature genes, we analyzed the transcriptomes of microglia isolated from stroke mice 24 h after MCAO compared to sham-operated controls. As expected, microglia showed a highly activated and proinflammatory phenotype (Figures S1A–S1C). We then compared the 3900 stroke-responsive genes (Figure S1B) with the 665 VB12-dependent genes (Figure 5B), which showed a negative correlation. The 246 stroke-repressed genes were upregulated by VB12, accounting for 64.5% of all genes enriched in the VB12 group (245 out of 380), while 141 stroke-activated genes (49.5% of downregulated genes) were found to be suppressed in VB12 mice (Figure 5C). In addition, VB12 mainly inhibited the expression of genes involved in inflammatory response (e.g., *Spp1*, *Cxcl3*, *Ecm1*, *Pla2g7*) and supported the sugar transporters (e.g., *Slc2a5*, *Slc5a10*), the M2 macrophage marker *Mrc2* and the synaptogenic factor catenin delta 2 (*Ctnnd2*) (Figure 5D). Furthermore, gene set enrichment analysis using the 386 VB12-regulated signature genes demonstrated that VB12 enhanced cell surface signaling and communication pathways, whereas its deficiency resulted in increased intracellular activities due to the enrichment of inflammatory effector genes (Figure 5E).

The β-catenin signaling pathway drives microglial anti-inflammatory activation and alleviates microglia-mediated neuroinflammation after ischemic stroke.[39,40] Here, we observed enriched β-catenin binding genes, including *Tcf7l2*, *Smad3*, and *Smad7*, which prevent β-catenin degradation[41] and stabilizing its binding[42] in microglia derived from VB12 mice (Figure 5F). In addition, microglia from VB12 mice demonstrated increased transcription of NF-κB inhibitors (*Nfkbia*, *Nfkbid*, and *Nfkbiz*), inhibitory *Siglec* family members (*Siglece*, *Siglecf*, and *Siglech*) and the transcription factor *Hhex*, all of which are involved in regulating inflammation-related genes in microglia.[43] Accordingly, VB12 reduced the expression of a number of genes involved in the activation of inflammatory microglia, including *Cd44*, *Ccr1*, *Cxcl2*, *Cxcl3*, and *Adam8*. Furthermore, we also observed enriched transcripts of mitochondrial-encoded genes (e.g., *mt-Co2*) in microglia from VB12 mice (Figure 5F). In contrast, the lipid metabolic process appeared to be dampened, as genes such as *Acot1*, *Acot2*, *Acadl*, and *Fabp5* were all reduced in VB12 mice. Intriguingly, the AP-1 transcription factors, including *Jun*, *Junb*, and *Fos*, which are known to promote microglial activation and drive a regulatory response to ischemic stroke,[44] were also activated by VB12, suggesting that VB12 transcriptionally programmed microglia to resist stroke-induced neuroinflammation.

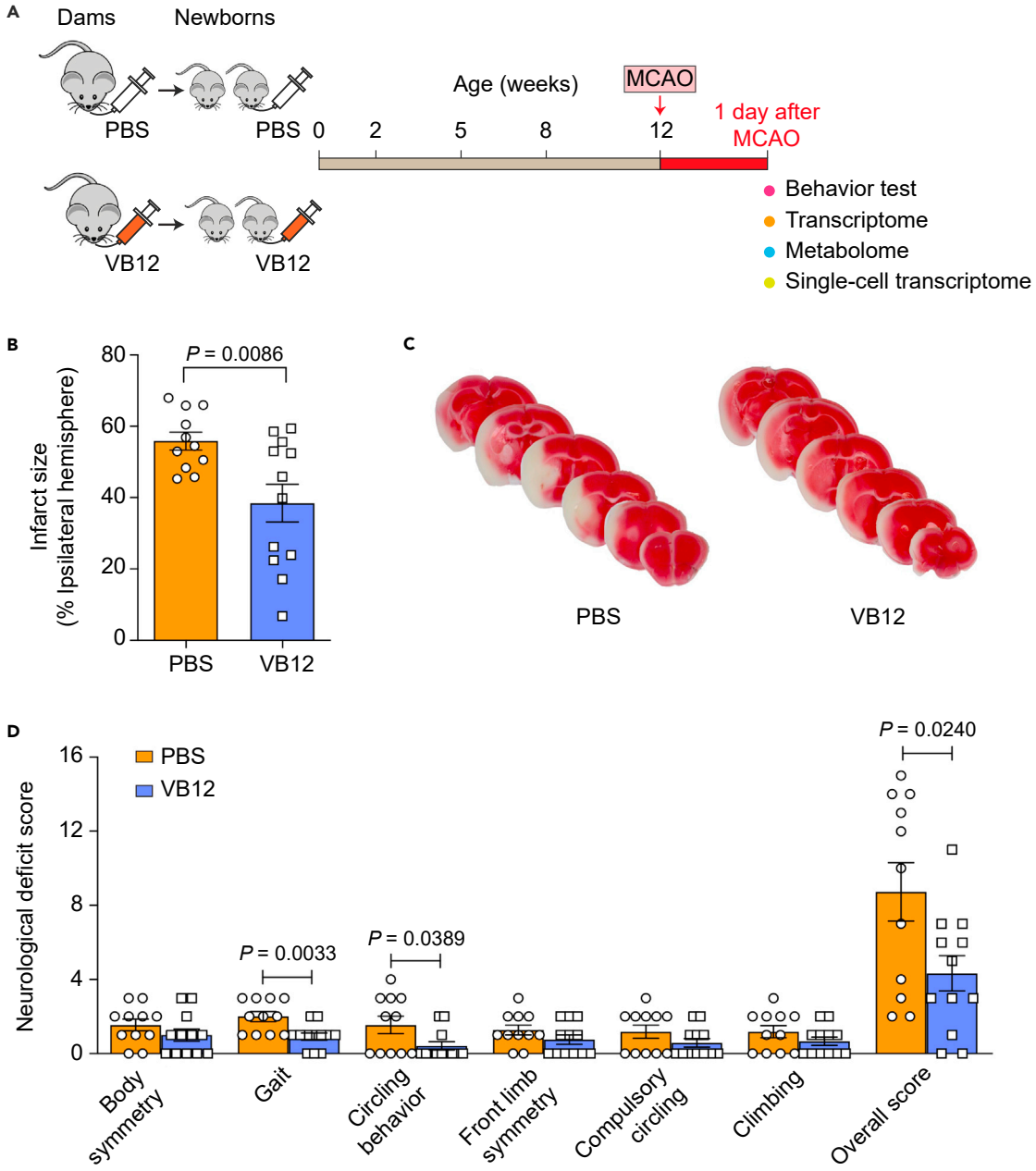

Figure 3. VB12-deficiency results in larger infarct size and worse neurological deficits following ischemic stroke

(A) Experimental scheme. C57schC57BL/6 mice kept on VB12-deficient diet were gavaged with VB12 or PBS for 12 weeks and then subjected to 45 min of middle cerebral artery occlusion (MCAO). Mice were euthanized 24 h after MCAO to isolate microglia for bulk RNA-seq, single-cell RNA-seq and metabolomic analysis. The neurological behavior of the mice was examined before the animals were euthanized.

(B) Increased infarct size in PBS-gavaged mice compared to VB12-gavaged mice (n = 11–12/group).

(C) Representative TTC-stained brain sections from PBS and VB12 groups.

(D) Neurological deficit scores across different functional domains, where a lower value indicates a better function. Statistics was determined by Unpaired *t*-test.

VB12 spatially and differentially regulates microglia at single-cell resolution

To examine the microglia heterogenicity during ischemic stroke, microglia were FACS-sorted from VB12 and control mice 1 day after stroke to perform single-cell transcriptomic analysis.[38] Here, a total of 37,729 cells isolated from 6 animals were sequenced at comparable sequencing depths (60,770–83,315 reads/cell) and had a similar median gene number (2,076–2,725) in all samples. To identify transcriptionally distinct microglial subpopulations, we performed dimensionality reduction and clustering, with 10 microglia subpopulations visualized by UMAP

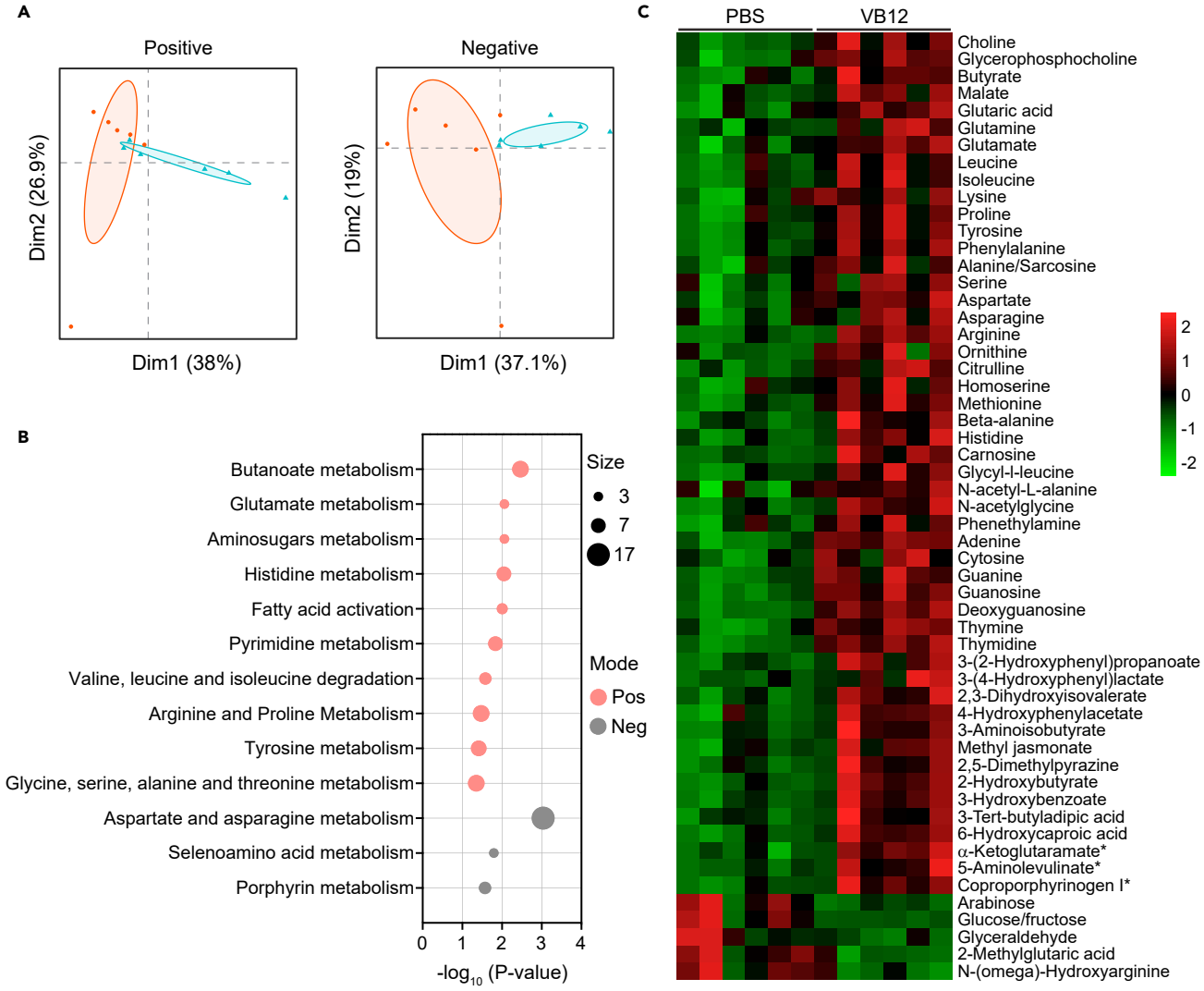

Figure 4. VB12 programs the metabolomes of microglia in response to ischemic stroke

(A) PCA plots of metabolite features in microglia FACS-sorted from VB12- and PBS-gavaged mice 24 h after MCAO (n = 6/group).

(B) Significant metabolic pathway between VB12 and PBS groups following ischemic stroke. The overlapped size indicates the number of significant metabolic features mapped to corresponding pathways.

(C) Heatmap depicting differentially enriched metabolites. Metabolites labeled with asterisks (*) were identified based on their enrichment in significant metabolic pathways and the *m/z* match.

and marked by the expression of microglial signature genes (Figures 6A and S2A). Notably, white matter-associated microglia (WAM) and gray matter-associated microglia (GAM)[28] were largely separated as primary microglial clusters by *Mmp12* and a group of proinflammatory genes (*Tnf*, *Il1a*, *Ccl2*, and *Ccl12*) (Figure S2B). Two clusters (WAM-Rps and GAM-Rps) were characterized by the upregulation of genes encoding ribosomal subunits and mitochondrial transcripts (Figure S2B), which are part of microglial responses to aging.[45] There was also an additional age-associated microglial cluster (IFN),[46] characterized by a high expression of interferon (IFN)-related genes (e.g., *Isg15*, *Ifitm3*). CNS-associated macrophages (CAM; also known as border-associated macrophages) were defined by the expression of *Mrc1*, *Pf4*, and *F13a1*. In addition, a subset of microglia (cluster Cdk14) was identified that shared WAM signature genes (e.g., *Vim*, *Lgals3*, *Ctsb*, *Cd63*) and expressed high levels of genes such as *Cdk14*, *Gab2*, *Malat1*, and *Tanc2* (Figure S2C). While WAMs showed enriched sets of genes related to cell redox and iron homeostasis, GAMs exhibited a highly inflammatory phenotype (Figure S2D). Microglia from the Cdk14 cluster resembled a neuron-associated gene profile (e.g., *Tanc2*) and were enriched with pathways for phosphorylation, potentially indicating their active implication in neuronal interactions (Figure S2D).

To define the cell type-specific response of microglia to VB12-deficiency during ischemic stroke, we subsequently performed a differential expression analysis across different cell subpopulations. VB12-deficiency spatially impaired the frequencies of microglial populations, as

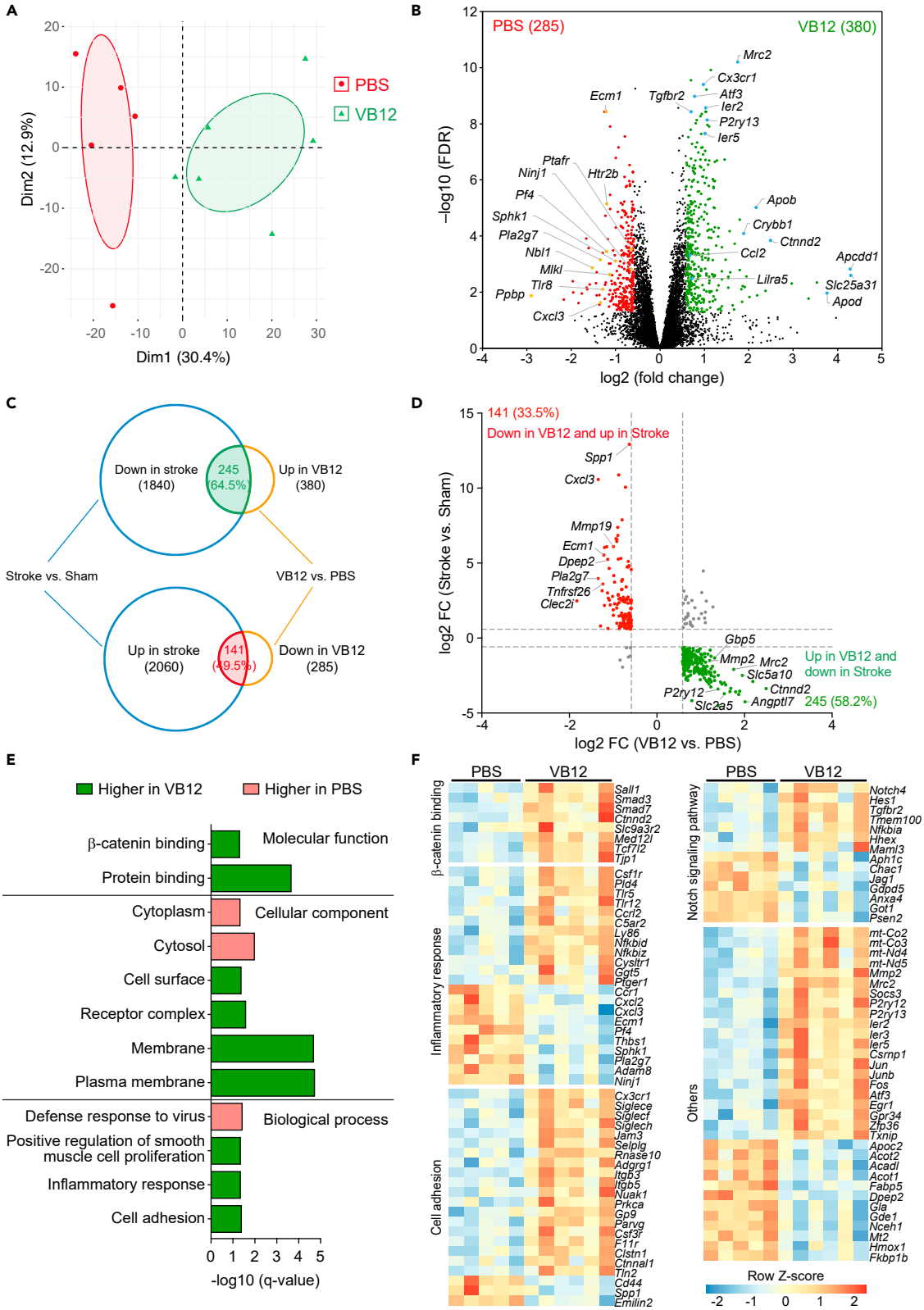
A
PBS
VB12
Dim2 (12.9%)
Dim1 (30.4%)
B
PBS (285)
VB12 (380)
−log10 (FDR)
log2 (fold change)
Mrc2
Cx3cr1
Ecm1
Tgfbr2
Atf3
Ier2
P2ry13
Ier5
Ptafr
Ninj1
Htr2b
Pf4
Sphk1
Pla2g7
Nbl1
Mlkl
Tlr8
Ppbp
Cxcl3
Apob
Crybb1
Ctnnd2
Ccl2
Apcdd1
Lilra5
Slc25a31
Apod
C
Down in stroke
(1840)
245
(64.5%)
Up in VB12
(380)
Stroke vs. Sham
VB12 vs. PBS
Up in stroke
(2060)
141
(29.5%)
Down in VB12
(285)
D
141 (33.5%)
Down in VB12 and up in Stroke
log2 FC (Stroke vs. Sham)
log2 FC (VB12 vs. PBS)
Spp1
Cxcl3
Mmp19
Ecm1
Dpep2
Pla2g7
Tnfrsf26
Clec2l
Gbp5
Mmp2
Mrc2
Slc5a10
Ctnnd2
P2ry12
Slc2a5
Angptl7
Up in VB12 and
down in Stroke
245 (58.2%)
E
Higher in VB12
Higher in PBS
β-catenin binding
Protein binding
Molecular function
Cytoplasm
Cytosol
Cell surface
Receptor complex
Membrane
Plasma membrane
Cellular component
Defense response to virus
Positive regulation of smooth
muscle cell proliferation
Inflammatory response
Cell adhesion
Biological process
-log10 (q-value)
F
PBS
VB12
β-catenin binding
Inflammatory response
Cell adhesion
Notch signaling pathway
Others
Sall1
Smad3
Smad7
Ctnnd2
Slc9a3r2
Med12l
Tcf7l2
Tjp1
Csf1r
Pld4
Tlr5
Tlr12
Ccrl2
C5ar2
Ly86
Nfkbid
Nfkbiz
Cysltr1
Ggt5
Ptger1
Ccr1
Cxcl2
Cxcl3
Ecm1
Pf4
Thbs1
Sphk1
Pla2g7
Adam8
Ninj1
Cx3cr1
Siglece
Siglecf
Siglech
Jam3
Selplg
Rnase10
Adgrg1
Itgb3
Itgb5
Nuak1
Prkca
Gp9
Parvg
Csf3r
F11r
Clstn1
Ctnnal1
Tln2
Cd44
Spp1
Emilin2
Notch4
Hes1
Tgfbr2
Tmem100
Nfkbia
Hhex
Maml3
Aph1c
Chac1
Jag1
Gdpd5
Anxa4
Got1
Psen2
mt-Co2
mt-Co3
mt-Nd4
mt-Nd5
Mmp2
Mrc2
Socs3
P2ry12
P2ry13
Ier2
Ier3
Ier5
Csrnp1
Jun
Junb
Fos
Atf3
Egr1
Gpr34
Zfp36
Txnip
Apoc2
Acot2
Acadl
Acot1
Fabp5
Dpep2
Gla
Gde1
Nceh1
Mt2
Hmox1
Fkbp1b
Row Z-score

Figure 5. VB12 programs the transcriptomes of microglial cells after ischemic stroke

(A) PCA plots of transcriptomes of microglia isolated from VB12- and PBS-gavaged mice (12 weeks old) 24 h after ischemic stroke (n = 5–6/group).

(B) Volcano plot showing differentially expressed genes (fold change>1.5, FDR<0.05) in microglia isolated from mice gavaged with VB12 versus PBS. The number of DEGs enriched in each group is shown in parentheses.

(C) Venn diagrams showing VB12 upregulated the stroke-suppressed DEGs and down-regulated stroke-activated DEGs in microglia. Note: a total of 1840 genes were downregulated, and 2060 genes were upregulated in microglia of mice 24 h post-stroke compared to sham-operated controls.

(D) Comparison of stroke-responsive and VB12-dependent microglia-enriched genes. Gene dots indicate genes downregulated by stroke but their expressions were supported when mice were gavaged with VB12. Red dots indicated genes activated by stroke but down-regulated by VB12 compared to PBS-gavaged mice.

(E) Gene set enrichment analysis using the 245 upregulated and 141 downregulated signature genes in microglia of VB12-gavaged mice after stroke.

(F) Heatmap of DEGs related to indicated pathways.

VB12-deficient mice appeared to have increased percentages of WAMs but reduced frequencies of GAMs (Figure 6B). Further, VB12 upregulated lipoprotein lipase (*Lpl*), which facilitates microglial lipid uptake and supports remyelination through the clearance of lipid debris,[47] and downregulated metallothioneins (*Mt1* and *Mt2*) induced by cell stress and ischemia,[48] as well as *Alox5ap* essential for leukotriene production, serving as a positive regulator of inflammation,[49] in most of the microglia subsets (Figure 6C). Although the frequency of WAMs was increased, inflammatory pathways, including chemokine and cellular response to bacterial lipopolysaccharides, were significantly downregulated in VB12 mice after stroke (Figure 6D). Accordingly, the inflammatory genes, including *Cxcl2*, *Lilrb4a*, and *Nlrp3*, were reduced in GAMs by VB12 (Figure 6E), whereas WAMs from VB12 mice showed increased expression of *Il1rn*, which counterbalances the inflammatory effects of IL-1,[50] *Cd72* that is involved in scavenging and recycling of lipid debris,[51] and *Csf1*, which promotes microglial survival.[52]

Furthermore, transcription factors involved in microglial activation and inflammation, including *Klf2*, *Jun* and *Rhob*, were suppressed in WAMs from VB12 mice. In contrast, activation of these transcription factors (e.g., *Fos*, *Jund*, *Junb*, *Atf3*) together with proinflammatory cytokines/chemokines (e.g., *Tnf*, *Il1a*, *Ccl3*, *Ccl12*) and antigen presentation molecules (e.g., *C1qa*, *C1qb*) (Figure 6E) was restricted to a specific microglial subset (Mmp12_Infla) from VB12-gavaged mice that expressed the marker genes of both WAMs and GAMs (Figure S2C). However, the frequencies of the Mmp12_Infla cluster was reduced from 5.9% in PBS on average to 2.6% in VB12-gavaged mice (Figure 6B), potentially indicating the compartmentalization of the inflammatory response in VB12 mice. Interestingly, VB12-supported mitochondrial activation was only observed in the Cdk14 cluster, which was also enriched in cell migration (*Cd9*) and activation genes (*Cd83*). However, the phagocytic function of microglia appeared to be tightly regulated as the expression of the intracellular engulfment protein *ELMO1*, which is critical for the clearance of apoptotic cells,[53] was tuned (Figure 6E), demonstrating that VB12 plays a crucial role in the proper control of microglial activation during ischemic stroke.

VB12 improves long-term neurobehavioral outcomes post-stroke

To further investigate the potential impact of VB12-deficiency on long-term stroke outcomes, we monitored the neurological behaviors of VB12 and PBS mice at different time points after stroke (Figure 7A). Here, VB12 mice showed a better survival rate (Figure 7B) and a significantly smaller infarct volume compared to VB12-deficient mice (Figures 7C and 7D). Furthermore, VB12 significantly alleviated stroke-induced neurological impairment (Figures 7E and 7F) and attenuated body weight loss on day 7 after stroke (Figure 7G). Although stroke resulted in significant impairment in locomotor function and muscle strength, no significant difference was observed in the total distance traveled in the open-field test or forepaws muscle strength (Figures S3A and S3E). However, the VB12 group showed much better recovery of sensorimotor function after stroke, as measured by a vertical grid test, than the PBS controls (Figures 7H and 7I). In addition, the novel object recognition (NOR) test revealed that VB12 mice showed much better recovery of long-term recognition memory performance than PBS controls 28 days after stroke (Figures 7J–7L), and that no significant difference in spatial memory recovery was observed between these two groups (Figures S3F and S3G).

To investigate whether the observed neurological improvement was dependent on functional microglia, these cells were depleted by feeding the CSF1R inhibitor PLX5622 to PBS and VB12 mice for 14 days. While kept on the PLX5622-containing diets, these mice were subjected to MCAO, and neurological behaviors were analyzed. Data demonstrated no neurological improvement in VB12-gavaged mice compared to PBS controls in the absence of microglia (Figures S4A and S4B), highlighting a crucial role of VB12-dependent microglia regulation in resisting stroke-associated neurological impairment. Altogether, our data strongly suggest that VB12 exerts beneficial effects on reducing infarct volume and improving long-term neurological deficits in the aftermath of an ischemic stroke.

DISCUSSION

Acute ischemic stroke can lead to rapid and irreversible deficits in motor ability, cognitive function, and death.[54,55] Increased efforts are urgently needed to significantly prevent stroke-induced neuroinflammation, ameliorate secondary neurologic damage, and improve neurologic recovery after ischemic stroke.[54] Thus, reprogramming reactive microglia, which are crucially involved in brain tissue damage, is of great interest. Microglia are activated as early as 24 h after acute ischemic stroke.[56] These cells release extremely high levels of inflammatory cytokines, reactive oxygen species, and matrix metalloproteinases and recruit circulating pathogenic T cells (e.g., $IL17^+$ γδ T cells) into the brain and meninges.[57] Following this acute neuroinflammatory phase, regulatory immune cascades must be activated to limit elaborated inflammatory neural injury. Despite the crucial role of neuroinflammation in perpetuating secondary brain injury, available immunosuppressive therapies have failed in clinical trials, possibly due to exacerbation of immunological dysfunction following ischemic stroke.[58] Thus, we asked

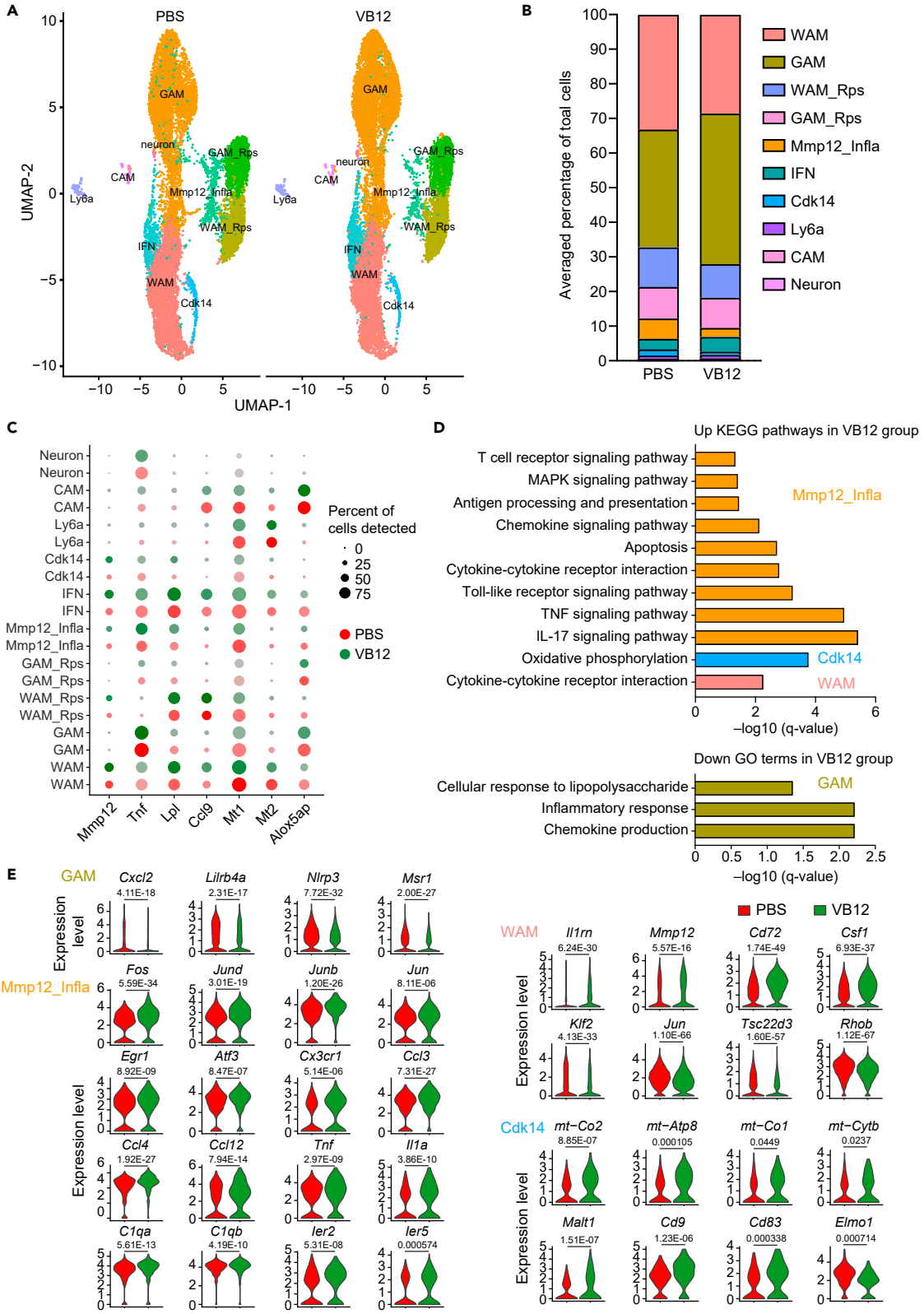
A
PBS
VB12
UMAP-2
UMAP-1
GAM
neuron
GAM_Rps
CAM
Ly6a
Mmp12_Infla
WAM_Rps
IFN
WAM
Cdk14
B
Averaged percentage of toal cells
WAM
GAM
WAM_Rps
GAM_Rps
Mmp12_Infla
IFN
Cdk14
Ly6a
CAM
Neuron
C
Neuron
CAM
Ly6a
Cdk14
IFN
Mmp12_Infla
GAM_Rps
WAM_Rps
GAM
WAM
Mmp12
Tnf
Lpl
Ccl9
Mt1
M2
Alox5ap
Percent of cells detected
PBS
VB12
D
Up KEGG pathways in VB12 group
T cell receptor signaling pathway
MAPK signaling pathway
Antigen processing and presentation
Chemokine signaling pathway
Apoptosis
Cytokine-cytokine receptor interaction
Toll-like receptor signaling pathway
TNF signaling pathway
IL-17 signaling pathway
Oxidative phosphorylation
Cytokine-cytokine receptor interaction
Mmp12_Infla
Cdk14
WAM
–log10 (q-value)
Down GO terms in VB12 group
Cellular response to lipopolysaccharide
Inflammatory response
Chemokine production
GAM
–log10 (q-value)
E
GAM
Mmp12_Infla
WAM
Cdk14
Expression level
PBS
VB12
Cxcl2
Lilrb4a
Nlrp3
Msr1
Fos
Jund
Junb
Jun
Egr1
Atf3
Cx3cr1
Ccl3
Ccl4
Ccl12
Tnf
Il1a
C1qa
C1qb
Ier2
Ier5
Il1rn
Mmp12
Cd72
Csf1
Klf2
Jun
Tsc22d3
Rhob
mt−Co2
mt−Atp8
mt−Co1
mt−Cytb
Malt1
Cd9
Cd83
Elmo1

Figure 6. VB12 differentially regulates microglial subpopulations to resist stroke-induced neuroinflammation

(A) Cell-type clusters split by conditions (PBS and VB12). We used uniform manifold approximation and projection (UMAP) to visualize the clustering (color coding) of 37,729 microglia isolated from VB12- and PBS-gavaged mice 24 h after MCAO (n = 3/group). GAM, gray matter-associated microglia; WAM, white matter-associated microglia; CAM, CNS-associated microglia.

(B) The averaged proportion of each cell type in PBS and VB12 groups.

(C) Dot plots depicting the expression of representative genes across different subpopulations between PBS and VB12 group.

(D) Gene ontology and KEGG pathways enriched in different cell subsets of PBS or VB12 group.

(E) Violin plots illustrating the expression of top differentially expressed genes in indicated microglia subsets. FDR-adjusted P-values are shown.

whether a crucial cofactor such as dietary VB12 may functionally contribute to microglial programs not only in homeostasis but also in post-stroke inflammation. Here, we demonstrate that compared to its deficiency, VB12 supports the transcriptional and metabolic activities of critical cellular programs implicated in microglial regulation to resist ischemic stroke-associated neuroinflammation, resulting in improved neurological function.

Mechanistically, following absorption and release of VB12 by iECs, VB12 enters the circulation to be captured by immune cells, including microglia expressing the receptor CD320.[59] Microglia utilize VB12 intracellularly to promote the enzymatic functions of methionine synthase and methylmalonyl-CoA mutase. However, the continuous exposure to VB12-deficiency may have a long-lasting effect on microglia development. Accordingly, our data demonstrated that VB12-deficiency indeed impaired the activation and phagocytic function of microglia at homeostasis. This may impact the microglial function during normal development, as proper activation of microglia is essential to maintaining synaptic pruning, a crucial tool for neuroplasticity through which synapses can be engulfed and eliminated by microglia.[25]

Furthermore, VB12-deficiency, which impairs the conversion of methionine into homocysteine, may also increase microglial activation and neuroinflammation in neuropathological conditions,[60,61] including ischemic stroke. While VB12 globally reduced the neuroinflammation and reversed the expression of stroke-associated gene signatures, different microglia subpopulations responded to VB12-deficiency in a manner that appeared to be specific to anatomic regions. For example, gray matter microglia in VB12-deficient mice showed greater activation of inflammatory pathways compared to WAM. Importantly, this activation was significantly impaired in VB12 mice. Notably, VB12 activated mitochondrial-encoded genes, particularly in the Cdk14 microglia cluster. Interestingly, our previous studies demonstrated the interplay of VB12 in crucially supporting mitochondrial respiration of iECs, which was coordinated by the gut microbiome and associated metabolites in the hosts.[19] However, it remains unclear how mitochondrial genes were only stimulated in a specific microglial subpopulation and whether the host microbiome physiology also contributes to such gene activation. Nevertheless, these data further signify the relevance of VB12 in selectively supporting the functions of microglial subsets. Possibly, a balanced immune regulation-immune activation circuit between microglial subsets during stroke may support vital neuroprotective signals necessary to alleviate collateral immune-mediated brain injury and stimulating neurorepair.

Accumulating evidence suggests that gut microbiome-associated metabolites can remotely support the protective physiology of brain cells.[62,63] Butyrate, produced by the gut microbiome, is involved in the neuroprotective function of microglia during ischemic stroke.[36,64] Notably, we have previously also demonstrated that VB12 critically modulated the functions of gut microbiota and enhanced butyrate production in the gut,[19] which can enter the systemic circulation to be subsequently absorbed and functionally suppress inflammatory microglial activation, as shown here through metabolomic analysis.

In conclusion, our results demonstrated that VB12 plays a crucial role in programming molecular and metabolic pathways of microglia to mitigate ischemic stroke-induced neuroinflammation resulting in improved neurological outcomes. Thus, controlling neuroinflammation potentiated by ischemic stroke through VB12-dependent intervention may represent a promising therapeutic target for future clinical settings.

Limitations of the study

Although we have demonstrated the differential effects of VB12 on microglia in general and microglial subpopulations in particular, how these different microglial subpopulations contribute to alleviating stroke-induced neuroinflammation remains to be further elucidated. Furthermore, we observed activation of mitochondrial gene expression in specific microglial clusters during ischemic stroke. Again, further studies are still needed to better understand whether mitochondrial respiration and metabolism are functionally maintained by VB12. Furthermore, the function of this specific cluster in the context of ischemic stroke requires further attention and investigation. Moreover, only 10–12 weeks old male mice were used in this study. Thus, it remains to be seen whether our funding also depends on gender and age-related factors. Additionally, a comprehensive study could be of crucial interest to investigate the effects of VB12 on the molecular and metabolic programs in microglia of stroke patients considering tissue restriction, which could significantly impede the studies.

STAR★METHODS

Detailed methods are provided in the online version of this paper and include the following:

- KEY RESOURCES TABLE
- RESOURCE AVAILABILITY
  - Lead contact
  - Materials availability

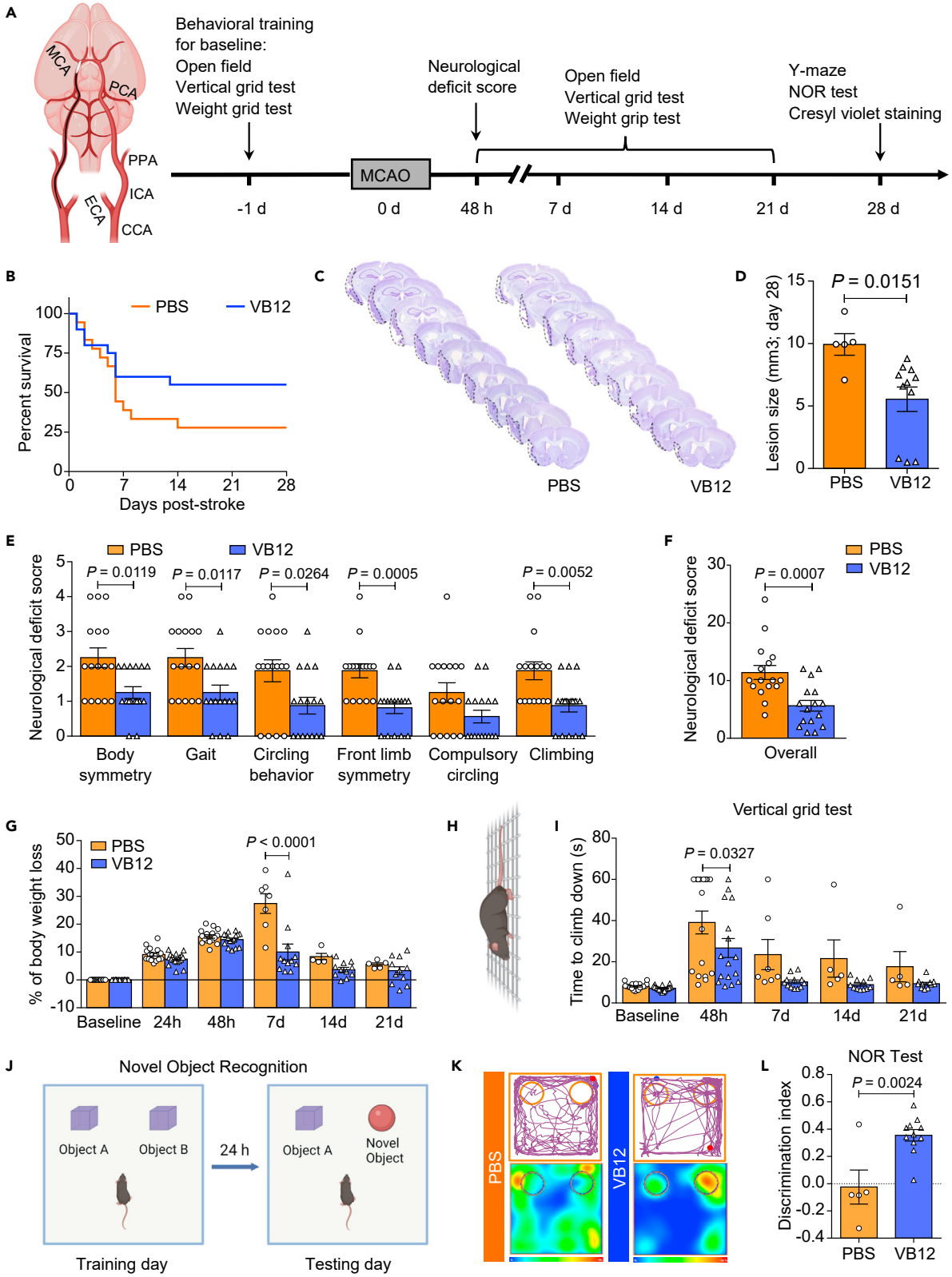
A
MCA
PCA
PPA
ICA
ECA
CCA
Behavioral training
for baseline:
Open field
Vertical grid test
Weight grid test
Neurological
deficit score
Open field
Vertical grid test
Weight grip test
Y-maze
NOR test
Cresyl violet staining
MCAO
-1 d
0 d
48 h
7 d
14 d
21 d
28 d
B
PBS
VB12
Percent survival
Days post-stroke
C
PBS
VB12
D
P = 0.0151
Lesion size (mm3; day 28)
PBS
VB12
E
PBS
VB12
P = 0.0119
P = 0.0117
P = 0.0264
P = 0.0005
P = 0.0052
Neurological deficit socre
Body symmetry
Gait
Circling behavior
Front limb symmetry
Compulsory circling
Climbing
F
PBS
VB12
P = 0.0007
Neurological deficit socre
Overall
G
PBS
VB12
P < 0.0001
% of body weight loss
Baseline
24h
48h
7d
14d
21d
H
I
Vertical grid test
P = 0.0327
Time to climb down (s)
Baseline
48h
7d
14d
21d
J
Novel Object Recognition
Object A
Object B
24 h
Object A
Novel Object
Training day
Testing day
K
PBS
VB12
L
NOR Test
P = 0.0024
Discrimination index
PBS
VB12

Figure 7. VB12 exerts beneficial effects on reducing infarct volume and improving long-term neurobehavioral outcomes in ischemic stroke mice

(A) Schematic drawings of the intraluminal filament MCAO surgery and the experimental timeline.

(B) Kaplan-Meier survival curve for 28-day survival in VB12-deficient mice gavaged with PBS or VB12 following transient MCAO.

(C and D) Representative images of Cresyl violet-stained brain sections and graphical data show that VB12-gavaged mice had a significantly smaller stroke volume than PBS-treated animals at 28 days after stroke.

(E and F) The VB12-gavaged mice exhibit a dramatically reduced neurological deficit scores compared to PBS controls.

(G) Body weight loss was recorded in VB12- and PBS-gavaged mice at different time points after stroke.

(H and I) No significant baseline difference was detected between PBS- and VB12-gavaged mice in the vertical grid test, but mice received VB12 exhibited much less time to climb down from the top of the apparatus than the PBS controls after ischemic stroke.

(J–L) Cognitive function was evaluated by novel object recognition (NOR) test. Representative tracking paths, heatmaps, and graphical data show that VB12-gavaged mice had much better recovery in long-term recognition memory performance than PBS controls at 28 days after stroke. two-way ANOVA with Bonferroni post-tests (G and H), Unpaired t-test (D and L), or Mann-Whitney test (E and F); N = 20/group were initially assigned to receive stroke surgery, and one mouse in the PBS group was excluded since it had no stroke. By the endpoint (day 28 after stroke) of the experiments, 14 mice in the PBS group and 9 mice in the VB12 group were dead.

SUPPLEMENTAL INFORMATION

Supplemental information can be found online at https://doi.org/10.1016/j.isci.2024.109480.

ACKNOWLEDGMENTS

This research was supported by NIH R01 DK109560, NIH R01 DK109560C, NIH R01AI154630-01, the Department of Veterans Affairs (VA) BX006310-01A to M.M and NIH R01 NS109816 to E.C.J.

AUTHOR CONTRIBUTIONS

M.M. directed the cellular and molecular studies and supervised data analyses. Y.G. performed cellular and molecular studies and bio-informatically analyzed the data. Y.G., C.Y., M.Z., J. L., and E.C.J. performed and supervised animal experiments. S.M.S., Y.D.L., H.S.J., B.F.D., and J.P. performed experiments. W.R. contributed to data discussion. Y.G., C.Y., W.R., E.C.J., and M.M. interpreted the data and wrote the manuscript. All the authors received the manuscript to review and offer comments before its submission to the journal.

DECLARATION OF INTERESTS

The authors declare no competing interests.

Received: November 24, 2023
Revised: December 14, 2023
Accepted: March 8, 2024
Published: March 14, 2024

REFERENCES

1. Kinlay, S. (2011). Changes in stroke epidemiology, prevention, and treatment. Circulation *124*, e494–e496.
2. Sevick, L.K., Ghali, S., Hill, M.D., Danthurebandara, V., Lorenzetti, D.L., Noseworthy, T., Spackman, E., and Clement, F. (2017). Systematic review of the cost and cost-effectiveness of rapid endovascular therapy for acute ischemic stroke. Stroke *48*, 2519–2526.
3. Gorelick, P.B. (2019). The global burden of stroke: persistent and disabling. Lancet Neurol. *18*, 417–418. https://doi.org/10.1016/S1474-4422(19)30030-4.
4. Kuriakose, D., and Xiao, Z. (2020). Pathophysiology and Treatment of Stroke: Present Status and Future Perspectives. Int. J. Mol. Sci. *21*, 7609. https://doi.org/10.3390/ijms21207609.
5. Roth, W., and Mohamadzadeh, M. (2021). Vitamin B12 and gut-brain homeostasis in the

pathophysiology of ischemic stroke. EBioMedicine *73*, 103676. https://doi.org/10.1016/j.ebiom.2021.103676.

6. House, A.A., Eliasziw, M., Cattran, D.C., Churchill, D.N., Oliver, M.J., Fine, A., Dresser, G.K., and Spence, J.D. (2010). Effect of B-vitamin therapy on progression of diabetic nephropathy: a randomized controlled trial. JAMA *303*, 1603–1609. https://doi.org/10.1001/jama.2010.490.
7. Bonaa, K.H., Njolstad, I., Ueland, P.M., Schirmer, H., Tverdal, A., Steigen, T., Wang, H., Nordrehaug, J.E., Arnesen, E., Rasmussen, K., and Investigators, N.T. (2006). Homocysteine lowering and cardiovascular events after acute myocardial infarction. N. Engl. J. Med. *354*, 1578–1588. https://doi.org/10.1056/NEJMoa055227.
8. Spence, J.D., Yi, Q., and Hankey, G.J. (2017). B vitamins in stroke prevention: time to reconsider. Lancet Neurol. *16*, 750–760. https://doi.org/10.1016/S1474-4422(17)30180-1.
9. Spence, J.D., Bang, H., Chambless, L.E., and Stampfer, M.J. (2005). Vitamin Intervention For Stroke Prevention trial: an efficacy analysis. Stroke *36*, 2404–2409. https://doi.org/10.1161/01.STR.0000185929.38534.f3.
10. Perea-Gomez, A., Cases, O., Lelièvre, V., Pulina, M.V., Collignon, J., Hadjantonakis, A.K., and Kozyraki, R. (2019). Loss of Cubilin, the intrinsic factor-vitamin B12 receptor, impairs visceral endoderm endocytosis and endodermal patterning in the mouse. Sci. Rep. *9*, 10168. https://doi.org/10.1038/s41598-019-46559-0.
11. Andersen, C.B.F., Madsen, M., Storm, T., Moestrup, S.K., and Andersen, G.R. (2010). Structural basis for receptor recognition of vitamin-B(12)-intrinsic factor complexes. Nature *464*, 445–448. https://doi.org/10.1038/nature08874.
12. Nielsen, M.J., Rasmussen, M.R., Andersen, C.B.F., Nexø, E., and Moestrup, S.K. (2012). Vitamin B12 transport from food to the body's cells–a sophisticated, multistep pathway. Nat. Rev. Gastroenterol. Hepatol. *9*, 345–354. https://doi.org/10.1038/nrgastro.2012.76.
13. Alam, A., Woo, J.S., Schmitz, J., Prinz, B., Root, K., Chen, F., Bloch, J.S., Zenobi, R., and Locher, K.P. (2016). Structural basis of transcobalamin recognition by human CD320 receptor. Nat. Commun. *7*, 12100. https://doi.org/10.1038/ncomms12100.
14. Lachner, C., Steinle, N.I., and Regenold, W.T. (2012). The neuropsychiatry of vitamin B12 deficiency in elderly patients. J. Neuropsychiatry Clin. Neurosci. *24*, 5–15. https://doi.org/10.1176/appi.neuropsych.11020052.
15. Stabler, S.P. (2013). Vitamin B12 deficiency. N. Engl. J. Med. *368*, 2041–2042. https://doi.org/10.1056/NEJMc1304350.
16. Akaike, A., Tamura, Y., Sato, Y., and Yokota, T. (1993). Protective effects of a vitamin B12 analog, methylcobalamin, against glutamate cytotoxicity in cultured cortical neurons. Eur. J. Pharmacol. *241*, 1–6. https://doi.org/10.1016/0014-2999(93)90925-8.
17. Simões, A.P., Silva, C.G., Marques, J.M., Pochmann, D., Porciúncula, L.O., Ferreira, S., Oses, J.P., Beleza, R.O., Real, J.I., Köfalvi, A., et al. (2018). Glutamate-induced and NMDA receptor-mediated neurodegeneration entails P2Y1 receptor activation. Cell Death Dis. *9*, 297. https://doi.org/10.1038/s41419-018-0351-1.
18. Ankarcrona, M., Dypbukt, J.M., Bonfoco, E., Zhivotovsky, B., Orrenius, S., Lipton, S.A., and Nicotera, P. (1995). Glutamate-induced neuronal death: a succession of necrosis or apoptosis depending on mitochondrial function. Neuron *15*, 961–973. https://doi.org/10.1016/0896-6273(95)90186-8.
19. Ge, Y., Zadeh, M., and Mohamadzadeh, M. (2022). Vitamin B12 coordinates ileal epithelial cell and microbiota functions to resist Salmonella infection in mice. J. Exp. Med. *219*, e20220057. https://doi.org/10.1084/jem.20220057.
20. Ge, Y., Zadeh, M., and Mohamadzadeh, M. (2022). Vitamin B12 Regulates the Transcriptional, Metabolic, and Epigenetic Programing in Human Ileal Epithelial Cells. Nutrients *14*, 2825. https://doi.org/10.3390/nu14142825.
21. Hankey, G.J. (2018). B vitamins for stroke prevention. Stroke Vasc. Neurol. *3*, 51–58.
22. Yahn, G.B., Abato, J.E., and Jadavji, N.M. (2021). Role of vitamin B12 deficiency in ischemic stroke risk and outcome. Neural Regen. Res. *16*, 470–474. https://doi.org/10.4103/1673-5374.291381.
23. Ginhoux, F., and Prinz, M. (2015). Origin of microglia: current concepts and past controversies. Cold Spring Harbor Perspect. Biol. *7*, a020537. https://doi.org/10.1101/cshperspect.a020537.
24. Michell-Robinson, M.A., Touil, H., Healy, L.M., Owen, D.R., Durafourt, B.A., Bar-Or, A., Antel, J.P., and Moore, C.S. (2015). Roles of microglia in brain development, tissue maintenance and repair. Brain *138*, 1138–1159. https://doi.org/10.1093/brain/awv066.
25. Paolicelli, R.C., Bolasco, G., Pagani, F., Maggi, L., Scianni, M., Panzanelli, P., Giustetto, M., Ferreira, T.A., Guiducci, E., Dumas, L., et al. (2011). Synaptic pruning by microglia is necessary for normal brain development. Science *333*, 1456–1458. https://doi.org/10.1126/science.1202529.
26. Yenari, M.A., Xu, L., Tang, X.N., Qiao, Y., and Giffard, R.G. (2006). Microglia potentiate damage to blood-brain barrier constituents: improvement by minocycline in vivo and in vitro. Stroke *37*, 1087–1093. https://doi.org/10.1161/01.STR.0000206281.77178.ac.
27. Szalay, G., Martinecz, B., Lénárt, N., Környei, Z., Orsolits, B., Judák, L., Császár, E., Fekete, R., West, B.L., Katona, G., et al. (2016). Microglia protect against brain injury and their selective elimination dysregulates neuronal network activity after stroke. Nat. Commun. *7*, 11499. https://doi.org/10.1038/ncomms11499.
28. Safaiyan, S., Besson-Girard, S., Kaya, T., Cantuti-Castelvetri, L., Liu, L., Ji, H., Schifferer, M., Gouna, G., Usifo, F., Kannaiyan, N., et al. (2021). White matter aging drives microglial diversity. Neuron *109*, 1100–1117.e10. https://doi.org/10.1016/j.neuron.2021.01.027.
29. Simopoulos, A.P. (2011). Evolutionary aspects of diet: the omega-6/omega-3 ratio and the brain. Mol. Neurobiol. *44*, 203–215. https://doi.org/10.1007/s12035-010-8162-0.
30. Fredholm, B.B., Chen, J.F., Masino, S.A., and Vaugeois, J.M. (2005). Actions of adenosine at its receptors in the CNS: insights from knockouts and drugs. Annu. Rev. Pharmacol. Toxicol. *45*, 385–412. https://doi.org/10.1146/annurev.pharmtox.45.120403.095731.
31. Wadhwa, M., Chauhan, G., Roy, K., Sahu, S., Deep, S., Jain, V., Kishore, K., Ray, K., Thakur, L., and Panjwani, U. (2018). Caffeine and Modafinil Ameliorate the Neuroinflammation and Anxious Behavior in Rats during Sleep Deprivation by Inhibiting the Microglia Activation. Front. Cell. Neurosci. *12*, 49. https://doi.org/10.3389/fncel.2018.00049.
32. Che, Y., Hou, L., Sun, F., Zhang, C., Liu, X., Piao, F., Zhang, D., Li, H., and Wang, Q. (2018). Taurine protects dopaminergic neurons in a mouse Parkinson's disease model through inhibition of microglial M1 polarization. Cell Death Dis. *9*, 435. https://doi.org/10.1038/s41419-018-0468-2.
33. Blusztajn, J.K., Liscovitch, M., and Richardson, U.I. (1987). Synthesis of acetylcholine from choline derived from phosphatidylcholine in a human neuronal cell line. Proc. Natl. Acad. Sci. USA *84*, 5474–5477. https://doi.org/10.1073/pnas.84.15.5474.
34. Feske, S.K. (2021). Ischemic Stroke. Am. J. Med. *134*, 1457–1464. https://doi.org/10.1016/j.amjmed.2021.07.027.
35. Czapski, G.A., and Strosznajder, J.B. (2021). Glutamate and GABA in Microglia-Neuron Cross-Talk in Alzheimer's Disease. Int. J. Mol. Sci. *22*, 11677. https://doi.org/10.3390/ijms222111677.
36. Patnala, R., Arumugam, T.V., Gupta, N., and Dheen, S.T. (2017). HDAC Inhibitor Sodium Butyrate-Mediated Epigenetic Regulation Enhances Neuroprotective Function of Microglia During Ischemic Stroke. Mol. Neurobiol. *54*, 6391–6411. https://doi.org/10.1007/s12035-016-0149-z.
37. Wallace, G.C., and Fukuto, J.M. (1991). Synthesis and bioactivity of N omega-hydroxyarginine: a possible intermediate in the biosynthesis of nitric oxide from arginine. J. Med. Chem. *34*, 1746–1748. https://doi.org/10.1021/jm00109a032.
38. Ge, Y., Zadeh, M., Yang, C., Candelario-Jalil, E., and Mohamadzadeh, M. (2022). Ischemic Stroke Impacts the Gut Microbiome, Ileal Epithelial and Immune Homeostasis. iScience *25*, 105437. https://doi.org/10.1016/j.isci.2022.105437.
39. Mo, Z., Zeng, Z., Liu, Y., Zeng, L., Fang, J., and Ma, Y. (2022). Activation of Wnt/Beta-Catenin Signaling Pathway as a Promising Therapeutic Candidate for Cerebral Ischemia/Reperfusion Injury. Front. Pharmacol. *13*, 914537. https://doi.org/10.3389/fphar.2022.914537.
40. Song, D., Zhang, X., Chen, J., Liu, X., Xue, J., Zhang, L., and Lan, X. (2019). Wnt canonical pathway activator TWS119 drives microglial anti-inflammatory activation and facilitates neurological recovery following experimental stroke. J. Neuroinflammation *16*, 256. https://doi.org/10.1186/s12974-019-1660-8.
41. Zhang, M., Wang, M., Tan, X., Li, T.F., Zhang, Y.E., and Chen, D. (2010). Smad3 prevents beta-catenin degradation and facilitates beta-catenin nuclear translocation in chondrocytes. J. Biol. Chem. *285*, 8703–8710. https://doi.org/10.1074/jbc.M109.093526.
42. Tang, Y., Liu, Z., Zhao, L., Clemens, T.L., and Cao, X. (2008). Smad7 stabilizes beta-catenin binding to E-cadherin complex and promotes cell-cell adhesion. J. Biol. Chem. *283*, 23956–23963. https://doi.org/10.1074/jbc.M800351200.
43. Sakate, R., Nishiyama, M., Fukuda, Y., Kitaoka, S., and Furuyashiki, T. (2022). The transcription factor Hhex regulates inflammation-related genes in microglia. J. Pharmacol. Sci. *149*, 166–171. https://doi.org/10.1016/j.jphs.2022.04.006.
44. Yenari, M.A., Kauppinen, T.M., and Swanson, R.A. (2010). Microglial activation in stroke: therapeutic targets. Neurotherapeutics *7*, 378–391. https://doi.org/10.1016/j.nurt.2010.07.005.

45. Ximerakis, M., Lipnick, S.L., Innes, B.T., Simmons, S.K., Adiconis, X., Dionne, D., Mayweather, B.A., Nguyen, L., Niziolek, Z., Ozek, C., et al. (2019). Single-cell transcriptomic profiling of the aging mouse brain. Nat. Neurosci. *22*, 1696–1708. https://doi.org/10.1038/s41593-019-0491-3.
46. Masuda, T., Sankowski, R., Staszewski, O., and Prinz, M. (2020). Microglia Heterogeneity in the Single-Cell Era. Cell Rep. *30*, 1271–1281. https://doi.org/10.1016/j.celrep.2020.01.010.
47. Loving, B.A., Tang, M., Neal, M.C., Gorkhali, S., Murphy, R., Eckel, R.H., and Bruce, K.D. (2021). Lipoprotein Lipase Regulates Microglial Lipid Droplet Accumulation. Cells *10*. https://doi.org/10.3390/cells10020198.
48. Manso, Y., Adlard, P.A., Carrasco, J., Vašák, M., and Hidalgo, J. (2011). Metallothionein and brain inflammation. J. Biol. Inorg. Chem. *16*, 1103–1113. https://doi.org/10.1007/s00775-011-0802-y.
49. Knight, A.C., Brill, S.A., Queen, S.E., Tarwater, P.M., and Mankowski, J.L. (2018). Increased Microglial CSF1R Expression in the SIV/Macaque Model of HIV CNS Disease. J. Neuropathol. Exp. Neurol. *77*, 199–206. https://doi.org/10.1093/jnen/nlx115.
50. Fearon, W.F., and Fearon, D.T. (2008). Inflammation and cardiovascular disease: role of the interleukin-1 receptor antagonist. Circulation *117*, 2577–2579. https://doi.org/10.1161/CIRCULATIONAHA.108.772491.
51. Zheng, K., Lin, L., Jiang, W., Chen, L., Zhang, X., Zhang, Q., Ren, Y., and Hao, J. (2022). Single-cell RNA-seq reveals the transcriptional landscape in ischemic stroke. J. Cerebr. Blood Flow Metabol. *42*, 56–73. https://doi.org/10.1177/0271678X211026770.
52. Barca, C., Foray, C., Hermann, S., Herrlinger, U., Remory, I., Laoui, D., Schäfers, M., Grauer, O.M., Zinnhardt, B., and Jacobs, A.H. (2021). The Colony Stimulating Factor-1 Receptor (CSF-1R)-Mediated Regulation of Microglia/Macrophages as a Target for Neurological Disorders (Glioma, Stroke). Front. Immunol. *12*, 787307. https://doi.org/10.3389/fimmu.2021.787307.
53. Lu, Z., Elliott, M.R., Chen, Y., Walsh, J.T., Klibanov, A.L., Ravichandran, K.S., and Kipnis, J. (2011). Phagocytic activity of neuronal progenitors regulates adult neurogenesis. Nat. Cell Biol. *13*, 1076–1083. https://doi.org/10.1038/ncb2299.
54. Hankey, G.J. (2017). Stroke. Lancet *389*, 641–654. https://doi.org/10.1016/S0140-6736(16)30962-X.
55. Grysiewicz, R.A., Thomas, K., and Pandey, D.K. (2008). Epidemiology of ischemic and hemorrhagic stroke: incidence, prevalence, mortality, and risk factors. Neurol. Clin. *26*, 871–895. vii. https://doi.org/10.1016/j.ncl.2008.07.003.
56. Morioka, T., Kalehua, A.N., and Streit, W.J. (1993). Characterization of microglial reaction after middle cerebral artery occlusion in rat brain. J. Comp. Neurol. *327*, 123–132. https://doi.org/10.1002/cne.903270110.
57. Candelario-Jalil, E., Dijkhuizen, R.M., and Magnus, T. (2022). Neuroinflammation, Stroke, Blood-Brain Barrier Dysfunction, and Imaging Modalities. Stroke *53*, 1473–1486. https://doi.org/10.1161/STROKEAHA.122.036946.
58. Elkind, M.S.V., Veltkamp, R., Montaner, J., Johnston, S.C., Singhal, A.B., Becker, K., Lansberg, M.G., Tang, W., Kasliwal, R., and Elkins, J. (2020). Natalizumab in acute ischemic stroke (ACTION II): a randomized, placebo-controlled trial. Neurology *95*, e1091–e1104.
59. Green, R., Allen, L.H., Bjørke-Monsen, A.L., Brito, A., Guéant, J.L., Miller, J.W., Molloy, A.M., Nexo, E., Stabler, S., Toh, B.H., et al. (2017). Vitamin B(12) deficiency. Nat. Rev. Dis. Prim. *3*, 17040. https://doi.org/10.1038/nrdp.2017.40.
60. Zou, C.G., Zhao, Y.S., Gao, S.Y., Li, S.D., Cao, X.Z., Zhang, M., and Zhang, K.Q. (2010). Homocysteine promotes proliferation and activation of microglia. Neurobiol. Aging *31*, 2069–2079. https://doi.org/10.1016/j.neurobiolaging.2008.11.007.
61. Chen, S., Dong, Z., Cheng, M., Zhao, Y., Wang, M., Sai, N., Wang, X., Liu, H., Huang, G., and Zhang, X. (2017). Homocysteine exaggerates microglia activation and neuroinflammation through microglia localized STAT3 overactivation following ischemic stroke. J. Neuroinflammation *14*, 187. https://doi.org/10.1186/s12974-017-0963-x.
62. Mohajeri, M.H., La Fata, G., Steinert, R.E., and Weber, P. (2018). Relationship between the gut microbiome and brain function. Nutr. Rev. *76*, 481–496. https://doi.org/10.1093/nutrit/nuy009.
63. Abdel-Haq, R., Schlachetzki, J.C.M., Glass, C.K., and Mazmanian, S.K. (2019). Microbiome-microglia connections via the gut-brain axis. J. Exp. Med. *216*, 41–59. https://doi.org/10.1084/jem.20180794.
64. Honarpisheh, P., Bryan, R.M., and McCullough, L.D. (2022). Aging Microbiota-Gut-Brain Axis in Stroke Risk and Outcome. Circ. Res. *130*, 1112–1144. https://doi.org/10.1161/CIRCRESAHA.122.319983.
65. Yang, C., Yang, Y., DeMars, K.M., Rosenberg, G.A., and Candelario-Jalil, E. (2020). Genetic Deletion or Pharmacological Inhibition of Cyclooxygenase-2 Reduces Blood-Brain Barrier Damage in Experimental Ischemic Stroke. Front. Neurol. *11*, 887. https://doi.org/10.3389/fneur.2020.00887.
66. Yang, C., Lavayen, B.P., Liu, L., Sanz, B.D., DeMars, K.M., Larochelle, J., Pompilus, M., Febo, M., Sun, Y.Y., Kuo, Y.M., et al. (2021). Neurovascular protection by adropin in experimental ischemic stroke through an endothelial nitric oxide synthase-dependent mechanism. Redox Biol. *48*, 102197. https://doi.org/10.1016/j.redox.2021.102197.
67. Butler, A., Hoffman, P., Smibert, P., Papalexi, E., and Satija, R. (2018). Integrating single-cell transcriptomic data across different conditions, technologies, and species. Nat. Biotechnol. *36*, 411–420. https://doi.org/10.1038/nbt.4096.
68. Li, S., Park, Y., Duraisingham, S., Strobel, F.H., Khan, N., Soltow, Q.A., Jones, D.P., and Pulendran, B. (2013). Predicting network activity from high throughput metabolomics. PLoS Comput. Biol. *9*, e1003123. https://doi.org/10.1371/journal.pcbi.1003123.
69. Liu, L., Yang, C., Lavayen, B.P., Tishko, R.J., Larochelle, J., and Candelario-Jalil, E. (2022). Targeted BRD4 protein degradation by dBET1 ameliorates acute ischemic brain injury and improves functional outcomes associated with reduced neuroinflammation and oxidative stress and preservation of blood-brain barrier integrity. J. Neuroinflammation *19*, 168. https://doi.org/10.1186/s12974-022-02533-8.
70. Glushakov, A.V., Robbins, S.W., Bracy, C.L., Narumiya, S., and Doré, S. (2013). Prostaglandin F2alpha FP receptor antagonist improves outcomes after experimental traumatic brain injury. J. Neuroinflammation *10*, 132. https://doi.org/10.1186/1742-2094-10-132.
71. Yang, C., Liu, L., Lavayen, B.P., Larochelle, J., Gunraj, R.E., Butler, A.A., and Candelario-Jalil, E. (2023). Therapeutic Benefits of Adropin in Aged Mice After Transient Ischemic Stroke via Reduction of Blood-Brain Barrier Damage. Stroke *54*, 234–244. https://doi.org/10.1161/STROKEAHA.122.039628.
72. Huang, Y., Xu, Z., Xiong, S., Sun, F., Qin, G., Hu, G., Wang, J., Zhao, L., Liang, Y.X., Wu, T., et al. (2018). Repopulated microglia are solely derived from the proliferation of residual microglia after acute depletion. Nat. Neurosci. *21*, 530–540. https://doi.org/10.1038/s41593-018-0090-8.

STAR★METHODS

KEY RESOURCES TABLE

REAGENT or RESOURCE	SOURCE	IDENTIFIER
Antibodies		
APC anti-mouse CD45	Thermo Fisher Scientific	Cat# 17-0451-82, RRID:AB_469392
APC/Cyanine7 anti-mouse/human CD11b	BioLegend	Cat# 101226, RRID:AB_830642
FITC anti-mouse CX3CR1	Thermo Fisher Scientific	Cat# 149020, RRID:AB_2565703
Chemicals, peptides, and recombinant proteins		
VB12 (cyanocobalamin)	Sigma-Aldrich	Cat# V2876
FcR Blocking Reagent	Miltenyi Biotec	Cat# 130-092-575
PowerUp SYBR Green Master Mix	Thermo Fisher Scientific	Cat# A25776
PLX5622 1200 ppm in VB12-deficient diet	Research Diets	N/A
Critical commercial assays		
LIVE/DEAD Fixable Violet Dead Cell Stain Kit	Thermo Fisher Scientific	Cat# L34964
RNeasy Plus Micro Kit	Qiagen	Cat# 74034
SMART-Seq HT Kit	Takara	Cat# 634438
Nextera XT DNA Library Preparation Kit	Illumina	Cat# FC-131-1096
IDT for Illumina DNA/RNA UD Indexes	Illumina	Cat# 20026121
Chromium Next GEM Single Cell 5′ Reagent Kits v2 (Dual Index)	10X Genomics	Cat# PN-1000263
Deposited data		
Bulk RNA-seq	This paper	NCBI BioProject PRJNA1018204
Single-cell RNA-seq	This paper	NCBI BioProject PRJNA1018264
Experimental models: Organisms/strains		
C56BL/6J mice (male)	Jackson Laboratory	https://www.jax.org/
Oligonucleotides		
See Table S1 for primers used in this study		
Software and algorithms		
Cell Ranger	10X Genomics	N/A
Seurat v4.0.6	Kinlay, et al [1]	https://satijalab.org/seurat/
GraphPad Prism 9	GraphPad	N/A
FlowJo v10	Treestar	N/A
Mummichog	Sevick, et al [2]	N/A
DAVID	Gorelick, et al [3]	https://david.ncifcrf.gov/
Other		
QuantStudio 6 Pro	Thermo Fisher Scientific	N/A
SH800S Cell Sorter	Sony	N/A
BD FACSAria™ Fusion Flow Cytometer	BD Biosciences	N/A
Chromium Controller	10X Genomics	N/A

RESOURCE AVAILABILITY

Lead contact

Further information and requests for resources and reagents should be directed to and will be fulfilled by the lead contact, Mansour Mohamadzadeh (Zadehm@uthscsa.edu).

Materials availability

This study did not generate new unique reagents.

Data and code availability

- Bulk RNA-seq and single-cell RNA-seq data have been made publicly available under the NCBI BioProject accession numbers PRJNA1018204 and PRJNA1018264, respectively. Accession numbers are listed in the key resources table.
- This study did not generate original code.
- Any additional information required to reanalyze the data reported in this paper is available from the lead contact upon request.

EXPERIMENTAL MODEL AND STUDY PARTICIPANT DETAILS

VB12-deficient C57BL/6 mice were obtained and maintained by feeding them a VB12-deficient diet (TD.180321; ENVIGO). Mice were kept on the VB12-deficient diet for at least two generations to fully deplete VB12. These mice were gavaged with VB12 (40 ng/mouse/twice a week before weaning and 400 ng/mouse/twice a week after weaning) for at least 2 generations to generate VB12-repleted mice, as previously described.[19] Subsequently, age-matched VB12- or PBS-gavaged male mice were used for experiments. All animal procedures complied with protocols approved by the Institutional Animal Care and Usage Committee (IACUC) of Laboratory Animal Resources of the University of Texas Health at San Antonio under protocol numbers 20210049AB and 20210065AR and the University of Florida under protocol number 202200000201.

METHOD DETAILS

Induction of transient focal cerebral ischemia

Transient focal cerebral ischemia was induced by intraluminal occlusion of the right middle cerebral artery (MCAO) for 45 min as our group described previously.[38,65] Briefly, mice were anesthetized by gas inhalation in a chamber containing 1.5-2% isoflurane in medical-grade oxygen. Once surgical levels of anesthesia were attained (assessed by the absence of hind leg withdrawal to pinch and level of response), animals were injected subcutaneously with 0.05 mg/kg of buprenorphine hydrochloride, and ophthalmic ointment was applied in the eyes. Body temperature was maintained at 37°C using a water-circulating heating pad (Gaymar, T/Pump) and temperature regulator with a rectal probe during surgery. The right common carotid artery (CCA), external carotid artery (ECA), and internal carotid artery (ICA) were exposed via a midline vertical incision in the anterior neck. A 12-mm-long 6-0 silicone-coated nylon filament (Doccol, Cat. No. 602134) was advanced gently into the ICA approximately 9-10 mm from the carotid bifurcation until mild resistance was felt, and cerebral blood flow (CBF) was reduced by at least 75% of the baseline value, as assessed by laser Doppler flowmetry (moorVMS-LDF1 blood flow monitor, Moor 556 Instruments). After 45 min of MCA occlusion, the filament was gently retracted to allow reperfusion (confirmed by laser Doppler). The skin was closed, anesthesia was discontinued, and the mice were allowed to recover in a temperature-controlled chamber (Thermocare ICS Warmer W-1 model 75W) set at 32°C. Once mice are recovered from anesthesia, they are placed in their home cages, and a heating pad (Snuggle Safe brand) is placed under the cage for the first 2 days after the stroke. Buprenorphine hydrochloride (0.05 mg/kg) is given subcutaneously every 12 hours for pain relief, along with 1.0 mL of warm saline. Sham-operated animals received the same surgical procedures except for the MCA occlusion.

Measurement of brain infarction by Cresyl violet staining

Brain infarction was measured by Cresyl violet staining as described in detail in our previous study.[66] Briefly, mice were euthanized 1 day or 28 days after stroke and transcardially perfused with 10 mL of saline containing 5 mM EDTA using a peristaltic pump at a speed of 5 mL/min, followed by 30 mL of 4% PFA in PBS. Brains were removed and post-fixed in 4% PFA for 24 hours, then transferred to PBS for storage at 4°C. Brains were cut into a series of 30-μm thick coronal sections on a semi-automated vibrating microtome (Compresstome® Model No. VF310-0Z; Precisionary Instruments, Natick, MA), and every tenth section throughout the infarct-containing region was stained using Cresyl violet (Cat. No. C5042, Sigma-Aldrich, St. Louis, MO, USA). Sections were scanned using an Aperio ScanScope® CS system and analyzed with ImageScope Software (Aperio Technologies, Vista, CA). The border between infarcted and non-infarcted areas was manually outlined for each section.

Isolation of microglia

Mice were perfused with PBS transcardially, and the forebrain was removed. Brains (ipsilateral hemisphere) were minced and enzymatically dissociated with 2 mg/ml collagenase D (Roche) and 0.3 mg/ml DNase I (Sigma) in RPMI-1640 medium (Gibco) supplemented with 10% fetal bovine serum (Gibco) for 45 min at 37°C. After digestion, tissues were passed through a syringe with a 21-gauge needle for 10 times and then transferred to a 40 mm cell strainer to make single-cell suspension. The cell suspension was then centrifuged and resuspended in 30% Percoll layered on 70% Percoll, and centrifuged at 2,500 rpm (about 1,285g) at 25°C for 30 min. Isolated cells were stained with a cocktail of fluorescent antibodies specific for APC-CD45 (Invitrogen, catalog 17-0451-83), APC-Cy7-CD11b (BioLegend, catalog 101226), FITC-CX3CR1 (BioLegend, catalog 149020). Dead cells were excluded using LIVE/DEAD Fixable Violet Dead Cell Stain (Invitrogen). $CD11b^{+}$ $CD45^{int}$ $CX3CR1^{+}$ microglia were sorted using a SONY SH800S or BD FACSAria Fusion cell sorter.

For metabolomic analysis, sorted cells were washed once with ice-cold PBS and cell pellets were stored at -80°C. Samples were shipped on dry ice to be processed; For bulk RNA-seq, cell pellets were suspended in RLT Plus buffer (Qiagen) and kept at −80°C until RNA isolation; For single-cell RNA-seq, sorted microglia were immediately used for GEM generation and barcoding following instructions of Chromium Next GEM Single Cell 5' Reagent Kits v2 (10X Genomics).

Bulk RNA-seq

Total RNA was extracted from FACS-sorted microglia isolated from each individual mouse using an RNeasy Plus Micro Kit (Qiagen). cDNA was generated using a SMART-Seq HT kit (Takara) and RNA-Seq libraries were constructed using a Nextera XT DNA Library Preparation Kit (Illumina). The barcoded RNA-seq libraries were sequenced on an Illumina NovaSeq 6000 system at the University of Florida ICBR NextGen DNA sequencing Core Facility. Obtained raw reads (2 x 150 bp) were aligned to the mouse reference genomes (GRCm38) using STAR v2.7.5c. Normalized counts (TPM) were generated using RSEM v1.3.3. DESeq2 was used to determine significantly expressed genes (DEGs) based on the criteria (TPM >1, FDR <0.05, fold change >1.5). Gene set enrichment analysis (GSEA) was performed using DAVID (https://david.ncifcrf.gov/).

Single-cell RNA-seq (scRNA-seq)

Microglia were FACS-purified from VB12- or PBS-gavaged mice one day after stroke. Cells (>75% viability) were processed using the Chromium single cell gene expression platform (10x Genomics) as described previously.[38] Microglia isolated from each mouse were directly loaded into each sample well following manufacturer's instructions and combined into droplets with barcoded beads using the Chromium controller (10X Genomics). The samples were sequenced on an Illumina NovaSeq 6000 s4 flow cell to generate 2x150 bp paired-end reads.

Sequence reads were processed using the Cell Ranger 6.0.1 pipeline and aligned to the GRCm38 (mm10) mouse reference genome. The exonic reads uniquely mapped to the transcriptome were then used for unique molecular identifier (UMI) counting. Using Seurat (v4.0.6) R package,[67] cells that contain fewer than 500 or more than 6000 genes (nFeature_RNA), less than 800 or more than 50,000 molecules (nCount_RNA), or more than 5% mitochondrial transcripts (percet.mt) were removed. Principal component analysis (PCA) was performed on the variable genes, and 50 principal components (PCs) were chosen based on elbow plots and jackstraw resampling. Samples of each condition were merged, and the two conditions (VB12 and PBS) were integrated using reciprocal PCA. Dimensionality reduction and visualization were performed with the UMAP algorithm, and unsupervised clustering of cells was performed using 50 PCs as defined above, with a resolution of 0.6. To identify signature genes of each cell cluster, the FindAllMarkers() function in Seurat was used with the following configurations: min.pct = 0.25, logfc.threshold = 0.585, only.pos = TRUE. An expression heatmap was generated for each sample by selecting the top 10 genes. To identify differentially expressed genes (DEGs) in each cell type across the two different conditions, the integrated Seurat object was split into different cell subpopulations using the subset() function and differential analysis was performed using FindMarkers() function. DEGs had adjusted P-values < 0.05 (corrected for multiple testing using the Bonferroni correction) and fold changes > 1.3.

qRT-PCR

For validating DEGs identified by RNA-Seq, quantitative real-time PCR was performed using cDNA samples from which RNA-seq libraries were constructed and the PowerUp SYBR Green Master Mix (Thermo Fisher) on a QuantStudio 6 Pro real-time PCR system (Thermo Fisher). The relative quantification ($2^{-\Delta Ct}$) was used to determine the expression level of the target genes normalized to *Gapdh*. Primers sequences are listed in Table S1.

Metabolomic analysis

Microglia (~100,000 cells) were homogenized and processed for metabolomic analysis as described previously.[19,20] Briefly, samples were run in both positive and negative ionization with a mass resolution of 35,000 at m/z 200. Feature alignment and curation were performed by MZmine. After normalizing to total ion chromatogram, intensities were tested for group significance using unpaired Student's *t*-test. Metabolites were identified by comparison to the metabolomic library of purified standards. Metabolic pathway analysis was performed using *Mummichog*.[68] The pathways represented by at least 2 significant metabolites in positive or negative mode are presented.

Neurobehavioral tests

Neurobehavioral tests, including neurological deficit score (NDS), open field, vertical grid test, weight grip test, Y-maze, and novel object recognition (NOR), were performed at defined time points to evaluate the sensorimotor function, spatial memory and cognitive function of ischemic stroke mice. At 48 hr after stroke, neurological deficits were assessed using a comprehensive 24-point NDS as described by our group and others.[69,70] The assessment included six individual tests (body symmetry, gait, circling behavior, front limb symmetry, compulsory circling, and climbing). Each test was performed blindly and scored from 0 for normal performance up to 4 points with increasing severity. The sum of scores from the six individual tests was reported as the overall NDS.

The open field test is used to assess spontaneous locomotor activity. Mice were individually placed in an open field chamber (40 × 40 × 40 cm) with grey sidewalls and were allowed to freely explore the arena for 10 min. The open field arena was cleaned with 70% ethanol between tests. The movements of the animals were automatically tracked with a video camera placed above the apparatus and analyzed using the ANY-maze software (Stoelting, Wood Dale, IL). The total distance traveled in the arena was analyzed.

The vertical grid test was performed to assess neuromuscular strength and motor coordination in rodents. The approach was described in detail in our recent study.[69] The vertical grid apparatus is an open frame (55 cm height × 8 cm wide × 5 cm depth) made of a wire mesh (0.8 cm × 0.8 cm) on the backside. It is vertically placed in a cage filled with bedding material. Mice were individually placed on the top of the wire mesh, facing downward, and were allowed to climb down to the cage. The total time to climb down was recorded. If the mouse failed while descending or could not climb down to the cage for 60 seconds, the performance was expressed as the maximum duration of 60 seconds. Each mouse performed 3 trials with at least 5 seconds intervals, and the average time of 3 trials was used for analysis.

The weight grip test was performed to assess the muscular strength of the forepaws of animals, slightly modified from our recent study.[71] Briefly, six different weights (weight-1: 16.2 g, weight-2: 30.4 g, weight-3: 44.6 g, weight-4: 58.2 g, weight-5: 71.4 g, and weight-6: 84.4 g) were prepared by attaching a metal mesh to stainless steel links (Figure S3C). The animals were held by the middle/base of the tail and allowed to grasp the first weight (16.2 g), lying on the benchtop. The timer starts when the animal grasps the metal mesh using its forepaws, and the animal is lifted until the steel links are clear off the bench. A cutoff time of 3 seconds was the criterion for a successful test. If the mouse could hold the first weight for 3 seconds, it was tested on the next, heavier weight until it could not hold the selected weight for 3 seconds or lift it. If the mouse dropped the weight in less than 3 seconds, the time the animal could hold the weight was recorded. The trial was terminated after testing three times for the weight the mouse could not lift. A final total score was calculated as a sum of the point of each weight the mouse holds multiplied by the time (second) it is held. Thus, a mouse holding weight-5 for 3 seconds and weight-6 for 1 second, is assigned a score of (1×3 + 2×3 + 3×3 + 4×3 + 5×3 + 6×1) = 51.

Spatial memory was assessed by a preference of rodents to explore novel rather than familiar places in a Y-maze, and the protocol was described in detail in our recent study.[71] The Y-maze apparatus (15 × 3 × 5 inches; San Diego Instruments) was made of beige ABS plastic with three identical arms positioned at equal angles. In the training/familiarization trial, mice were individually allowed to explore two of the three arms for a total of 5 min while the third ('novel') arm was blocked and then returned to their home cage. After 60 min, the mice were placed back in the maze for 5 min with all three arms open. The apparatus was cleaned between trials with 70% ethanol. Time spent in each arm was automatically determined using the ANY-maze software with a camera fixed on the ceiling above the Y-maze apparatus. The time in the novel arm (%) was defined as the time spent in the novel arm divided by the time spent in all arms in the test trial and used to evaluate the spatial memory performance of the experimental animals.

The novel object recognition (NOR) test was performed to evaluate long-term recognition memory function as described in detail in our recent studies.[66,71] Briefly, for the training session, mice were individually placed in an open field chamber (40 × 40 × 40 cm) with grey sidewalls containing two identical objects for 8 minutes and returned to their home cage. After 24 hours, the mice were exposed to the familiar arena in the presence of the original object and a novel object to test long-term recognition memory for another 8 min. During the 8 min test session, the time spent exploring each object was recorded. The discrimination of recognition novelty was determined as a discrimination index: (time exploring the new object − time exploring the old object)/ (total time exploring both objects). Movements of animals were videotaped by an overhead camera and analyzed using the ANY-maze software.

Depletion of microglia by PLX5622

To deplete microglia, age-matched VB12- or PBS-gavaged mice (male, 10-12 weeks old) were fed VB12-deficient diet containing the CSF1R inhibitor PLX5622 (Research Diets) at 1200 PPM (1200 mg/kg of chow), beginning 2 weeks prior to MCAO surgery and continued until the end of the experiments.[72]

QUANTIFICATION AND STATISTICAL ANALYSIS

Statistical analyses were performed using GraphPad Prism v9.1.2. Prior to statistical analysis, normality was tested using the Shapiro-Wilk normality test. Where the groups follow a Gaussian distribution, two-tailed unpaired Student's *t* test was performed. Where the groups did not follow a Gaussian distribution, Mann–Whitney *U* test was performed. $P < 0.05$ were considered as significant: $*P < 0.05$, $**P < 0.01$, $***P < 0.001$, $****P < 0.0001$.